Title:
Solar Occultation Satellite Data and Derived Meteorological Products: Sampling Issues and Comparisons with Aura MLS.

Submitted to: JGR-Atmospheres

Author list w/ email addresses:

Gloria Manney	manney@mls.jpl.nasa.gov
William H. Daffer	William.H.Daffer@jpl.nasa.gov
Joseph. M. Zawodny	Joseph.M.Zawodny@nasa.gov
Peter F. Bernath	pfb500@york.ac.uk
Karl W. Hoppel	Karl.Hoppel@nrl.navy.mil
Kaley A. Walker	kwalker@atmosp.physics.utoronto.ca
Brian W. Knosp	brian.knosp@jpl.nasa.gov
Chris Boone	cboone@acebox.uwaterloo.ca
Ellis E. Remsberg	Ellis.E.Remsberg@nasa.gov
Michelle L. Santee	mls@mls.jpl.nasa.gov
V. Lynn Harvey	lynn.harvey@lasp.colorado.edu
Steven Pawson	Steven.Pawson-1@nasa.gov
David R. Jackson	David.Jackson@metoffice.gov.uk
Lance Deaver	l.e.deaver@gats-inc.com
Hugh C. Pumphrey	H.C.Puphrey@ed.ac.uk
Alyn Lambert	alyn.lambert@jpl.nasa.gov
Michael J. Schwartz	Michael@mls.jpl.nasa.gov
Lucien Froidevaux	Lucien@mls.jpl.nasa.gov
Sean McLeod	sdmcleod@uwaterloo.ca
Lawrence L. Takacs	ltakacs@gmao.gsfc.nasa.gov
Max J. Suarez	Max.J.Suarez@nasa.gov
Charles R. Trepte	Charles.R.Trepte@nasa.gov
Nathaniel Livesey	livesey@mls.jpl.nasa.gov
Robert S. Harwood	rharwood@staffmail.ed.ac.uk
Joe W. Waters	joe@mls.jpl.nasa.gov

Abstract:

Derived Meteorological Products (DMPs, including potential temperature (θ), potential vorticity, equivalent latitude (EqL), horizontal winds and tropopause locations) have been produced for the locations and times of measurements by several solar occultation (SO) instruments and the Aura Microwave Limb Sounder (MLS). DMPs are calculated from several meteorological analyses for the Atmospheric Chemistry Experiment-Fourier Transform Spectrometer, Stratospheric Aerosol and Gas Experiment II and III, Halogen Occultation Experiment, and Polar Ozone and Aerosol Measurement II and III SO instruments and MLS. Time-series comparisons of MLS version 1.5 and SO data using DMPs show good qualitative agreement in time evolution of O_3, N_2O, H_2O, CO, HNO_3, HCl and temperature; quantitative agreement is good in most cases. EqL-coordinate comparisons of MLS version 2.2 and SO data show good quantitative agreement throughout the stratosphere for most of these species, with significant biases for a few species in localized regions. Comparisons in EqL coordinates of MLS and SO data, and of SO data with geographically coincident MLS data provide insight into where and how sampling effects are

1

important in interpretation of the sparse SO data, thus assisting in fully utilizing the SO data in scientific studies and comparisons with other sparse datasets. The DMPs are valuable for scientific studies and to facilitate validation of non-coincident measurements.

Popular Summary

This paper is associated with comparisons of sparse space-based observations of the structure of Earth's middle atmosphere.

Solar occultation techniques provide a method of obtaining highly accurate profile information on temperature and trace gases in the middle atmosphere. The method involves looking at the sun on layers of near-horizontal paths through the atmosphere, including one view of the sun above the atmosphere, which provides a means of calibration for the observing instrument. This opportunity to obtain the unimpeded view of the sun on each profile is one of the reasons for the high accuracy of the technique, because this knowledge can be used to continually correct for changes in solar output at the wavelengths observed and for any drifts in instrument performance.

A disadvantage of solar occultation techniques is that they tend to provide very sparse data, with only several tens of profiles per day. This means that cross-validation of data from platforms in different orbits is complicated because of lack of spatio-temporal coincidence of these observations. Sophisticated interpolation techniques are necessary to obtain meaningful comparisons between instruments. They are also needed to complete chemical budgets, if (for example) some constituents are observed from one platform while other related gases are observed from a different platform.

One technique for validation is to use meteorological analyses to establish "regimes" where the constituent measurements are likely to be related to each other. This approach relies on some reasonable assumptions about correlations among different gases, which are borne out by the fact that long-lived trace gases, whose distributions are primarily determined by local transport, correlate well when the correlation is performed on "material" surfaces. These surfaces, which are potential temperature in the vertical and potential vorticity in the horizontal, allow the trace gas distributions to be compiled effectively as latitude-height distributions in potential-temperature/potential-vorticity space. The potential vorticity component is converted to "equivalent latitude" which is that latitude that each potential vorticity contour would enclose if it were distributed symmetrically around the globe.

This paper presents a thorough validation of measurements from a number of solar occultation instruments, using "derived meteorological products" (the potential temperature and potential vorticity) from Goddard Earth Observing System, Version 5 (GEOS-5) and other meteorological analyses. Data from the limb-sounding Microwave Limb Sounder (MLS) on NASA's EOS-Aura platform are also used. The results reveal generally very good agreement among the MLS data and SO datasets, with some anomalies for specific gases in certain regions of the atmosphere. These results attest not only to the quality of the observations, but also to the physical robustness of the GEOS-5 and other meteorological analyses.

Solar Occultation Satellite Data and Derived Meteorological Products: Sampling Issues and Comparisons with Aura MLS

Gloria L. Manney[1,2], William H. Daffer[3], Joseph M. Zawodny[4], Peter F. Bernath[5,6], Karl W. Hoppel[7], Kaley A. Walker[5,8], Brian W. Knosp[1], Chris Boone[5], Ellis E. Remsberg[4], Michelle L. Santee[1], V. Lynn Harvey[9], Steven Pawson[10], David R. Jackson[11], Lance Deaver[12], Hugh C. Pumphrey[13], Alyn Lambert[1], Michael J. Schwartz[1], Lucien Froidevaux[1], Sean McLeod[5], Lawrence L. Takacs[10], Max J. Suarez[10], Charles R. Trepte[4], Nathaniel J. Livesey[1], Robert S. Harwood[13], and Joe W. Waters[1]

Abstract. Derived Meteorological Products (DMPs, including potential temperature (θ), potential vorticity, equivalent latitude (EqL), horizontal winds and tropopause locations) have been produced for the locations and times of measurements by several solar occultation (SO) instruments and the Aura Microwave Limb Sounder (MLS). DMPs are calculated from several meteorological analyses for the Atmospheric Chemistry Experiment-Fourier Transform Spectrometer, Stratospheric Aerosol and Gas Experiment II and III, Halogen Occultation Experiment, and Polar Ozone and Aerosol Measurement II and III SO instruments and MLS. Time-series comparisons of MLS version 1.5 and SO data using DMPs show good qualitative agreement in time evolution of O_3, N_2O, H_2O, CO, HNO_3, HCl and temperature; quantitative agreement is good in most cases. EqL-coordinate comparisons of MLS version 2.2 and SO data show good quantitative agreement throughout the stratosphere for most of these species, with significant biases for a few species in localized regions. Comparisons in EqL coordinates of MLS and SO data, and of SO data with geographically coincident MLS data provide insight into where and how sampling effects are important in interpretation of the sparse SO data, thus assisting in fully utilizing the SO data in scientific studies and comparisons with other sparse datasets. The DMPs are valuable for scientific studies and to facilitate validation of non-coincident measurements.

[1] Jet Propulsion Laboratory, California Institute of Technology, Pasadena, California, USA.

[2] Also at New Mexico Institute of Mining and Technology, Socorro, New Mexico, USA.

[3] Columbus Technologies and Services Inc., Pasadena, California, USA

[4] NASA Langley Research Center, Hampton, Virginia, USA.

[5] University of Waterloo, Waterloo, Ontario, Canada.

[6] University of York, Heslington, York, United Kingdom.

[7] Naval Research Laboratory, Washington, DC, USA.

[8] University of Toronto, Toronto, Ontario, Canada.

[9] LASP, University of Colorado, Boulder, Colorado, USA.

[10] NASA Goddard Space Flight Center, Greenbelt, Maryland, USA.

[11] Met Office, Exeter, United Kingdom.

[12] GATS, Inc., Hampton, Virginia, USA.

[13] University of Edinburgh, Edinburgh, United Kingdom.

1. Introduction

The characterization of atmospheric observations by air mass properties, such as location with respect to the stratospheric polar vortex or the tropopause, is an invaluable tool in numerous analyses, both for research studies and validation. It is especially valuable, and has been widely used, in studies using solar occultation (SO) satellite data, which consist of no more than 15 profiles per day at each of two latitudes. *Butchart and Remsberg* [1986] and *Lait et al.* [1990] mapped atmospheric trace gases with respect to potential vorticity (PV) and equivalent latitude (EqL, the latitude that would enclose the same area between it and the

pole as a given PV contour, *Butchart and Remsberg* [1986]). *Manney et al.* [1999] used PV and EqL with satellite data to enable detailed study of polar vortex dynamics and associated transport in ATMOS (Atmospheric Trace Molecule Spectroscopy) data from the ATLAS (Atmospheric Laboratory for Applications and Science) space-shuttle missions; a number of other studies of ATMOS, Halogen Occultation Experiment (HALOE), Polar Ozone and Aerosol Measurement (POAM) II and III, and Stratospheric Aerosol and Gas Experiment (SAGE) II and III data [*Schoeberl et al.*, 1995; *Randall et al.*, 2005, and references therein] have used EqL or PV to help realize the full "condition-space" coverage of the sparse SO datasets. Other studies of limb-sounding datasets, such as the Microwave Limb Sounder (MLS) instruments on the Upper Atmosphere Research Satellite (UARS) and Earth Observing System (EOS) Aura missions, have used PV or EqL mapping to study polar vortex dynamics and trace gas evolution [*Manney et al.*, 1995a, 2005a, and references therein].

Air mass characterization also facilitates comparisons using measurements that are geographically sparse and may not fulfill traditional coincidence criteria based on close matching of time and location. *Santee et al.* [2007a, b, this issue] use EqL as a coordinate to compare Aura MLS data with Upper Atmosphere Research Satellite (UARS) MLS measurements taken in the 1990s. EqL and PV mapping have been used in studies of aircraft and ground-based observations [e.g., *Lait et al.*, 1990; *Redaelli et al.*, 1994]. *Manney et al.* [2001] used EqL mapping, standard geographical coincidence criteria augmented by PV matching, and trajectory histories to compare ozone from seven instruments during the November 1994 period of the ATLAS-3 mission, including four SO instruments (ATMOS, HALOE, SAGE II and POAM II). PV or EqL can be used to augment or replace conventional coincidence criteria [e.g., *Michelsen et al.*, 2002; *Lumpe et al.*, 2003; *Thomason et al.*, 2006].

Several SO datasets are available for validation of Aura measurements, including HALOE, SAGE II and III, POAM III, and the Atmospheric Chemistry Experiment Fourier Transform Spectroscopy (ACE-FTS) instrument. To facilitate non-coincident validation and intercomparison of measurements sorted by air-mass characteristics, and for use in research studies combining Aura with SO datasets, a set of "derived meteorological products" (DMPs) has been calculated for these SO datasets; the DMPs consist of fields derived from the meteorological analyses' winds and temperatures, such as PV and EqL, and fields from the meteorological analyses, all interpolated to the locations and time of the satellite observations. DMPs have also been calculated for Aura MLS version 1.5 (v1.5) and version 2.2 (v2.2) datasets; as well as contributing to validation and sci-

ence studies, these are used in producing plots for routine inspection of MLS data, and daily EqL/potential temperature (θ) cross-sections that are posted on the MLS website [http://mls.jpl.nasa.gov]. In the following, we document the DMPs for the SO instruments and MLS and use them for comparisons of SO and MLS data. We explore effects of the satellites' different sampling and extend more traditional intercomparisons for validation. DMPs for MLS and/or SO instruments are also used in validation and comparisons in other papers in this issue [*Pawson et al.*, 2007; *Santee et al.*, 2007a, b].

2. Dataset Descriptions

2.1. Solar Occultation Datasets

2.1.1. ACE-FTS SCISAT-1, otherwise known as the Atmospheric Chemistry Experiment (ACE) [*Bernath et al.*, 2005] was launched August 2003. The primary instrument is the ACE-FTS (hereinafter referred to as ACE), a Fourier transform spectrometer featuring high resolution (0.02 cm^{-1}, corresponding to a ±25 cm maximum optical path difference) and broad spectral coverage in the infrared (750-4400 cm^{-1}). ACE works primarily in the solar occultation mode, collecting atmospheric limb measurements using the sun as a radiation source. Version 2.2 of the ACE retrievals [*Boone et al.*, 2005] is used here, except for O$_3$, for which the ACE product known as "version 2.2 ozone update" is used. Early validation efforts with the ACE data identified a roughly 10% low bias for altitudes near the O$_3$ concentration peak when compared to other satellite measurements [*Walker et al.*, 2005; *Fussen et al.*, 2005; *Petelina et al.*, 2005]. Version 2.2 processing uses microwindows in two spectroscopic regions: 1000-1150 cm^{-1} and 1800-2150 cm^{-1}. Version 2.2 O$_3$ update uses microwindows in the 950-1150 cm^{-1} range and, in preliminary comparisons, exhibits improved agreement with other datasets near the O$_3$ concentration peak. ACE vertical resolution is $\sim$3–4 km. Latitudes of measurements vary over an annual cycle with coverage as high as $\pm85°$ and an emphasis on the polar regions in winter and spring. Separate files with ACE geolocation information, primarily latitude and longitude as a function of altitude, are provided for each occultation; for occultations with missing geolocation files, the geolocation information is taken from the headers of the data files, which give 30-km tangent point latitude and longitude values; most differences are small, but can be up to $\sim$3° latitude and $\sim$10° longitude for brief periods, depending on the viewing geometry.

2.1.2. HALOE HALOE [*Russell et al.*, 1993] was operational on the Upper Atmosphere Research Satellite (UARS) from October 1991 through November 2005.

HALOE observations take approximately one month to cover the full range of latitudes sampled (ranging from $\pm 80°$ to $\pm 50°$, depending on season, reaching highest (lowest) latitudes in summer (winter)). Estimates of uncertainties for the profiles of the retrieved HALOE parameters from its first public release dataset (Version 17) are provided in *Journal of Geophysical Research, Atmospheres, 101, D6* – a special UARS Validation Issue published in 1996. The data used here are Version 19. Some updated uncertainty estimates for Version 19 are available for O_3 [*Randall et al.*, 2003], H_2O [*Kley et al.*, 2000], and temperature *Remsberg et al.* [2002]. Vertical resolution is ~ 2 km for O_3 and H_2O, ~ 3–4 km for temperature, and ~ 4 km for HCl. Temperatures in the HALOE files below 35 km are from the NCEP/CPC meteorological analyses. HALOE latitude and longitude as a function of height are provided on the same 0.3-km grid used for the temperature files.

2.1.3. POAM POAM II [*Glaccum et al.*, 1996] and POAM III [*Lucke et al.*, 1999] were visible/near-infrared solar occultation instruments that typically made 14-15 measurements per day in each hemisphere around a circle of latitude with a longitudinal spacing of about 25°. The latitudinal coverage was identical each year, slowly varying between 54°N - 71°N and 65°S - 88°S. POAM II obtained data from October 1993 until November 1996, when the host satellite failed; POAM III obtained data from late April 1998 through early December 2005. POAM II provided measurements of O_3, aerosol extinction, and NO_2; POAM III provided H_2O in addition to these. The POAM III Version 4 ozone retrievals differ little from the Version 3 retrievals described by *Lumpe et al.* [2002], and validated by *Lumpe et al.* [2003] and *Randall et al.* [2003]. At 15 km and above, the O_3 retrievals have a vertical resolution of ~ 1 km and an estimated precision of 5% [*Lumpe et al.*, 2002]. The H_2O retrievals extend from 5 to 50 km with 5-7% precision and a vertical resolution ranging from 1 km in the lower stratosphere to 3 km in the upper stratosphere. The H_2O retrievals have been validated by *Lumpe et al.* [2006]. Geolocation information (latitude, longitude and line-of-sight (LOS) angle) for POAM III were calculated on an 8-km grid, and interpolated linearly to the POAM 1-km measurement grid.

2.1.4. SAGE II SAGE II [http://science.hq.nasa.gov/missions/satellite_45.htm] used radiances at 600 nm to derive O_3 and at 940 nm to derive H_2O; it took measurements from October 1984 through August 2005. The instrument and earlier versions of the retrieval algorithm, as well as O_3 validation, are discussed by *Chu et al.* [1989], *Cunnold et al.* [1989], and *McCormick et al.* [1989]. SAGE II data used here are Version 6.2. O_3 data have ~ 1 km or less vertical resolution, and H_2O data no better than ~ 1 km. Validation of v6.2 O_3 and H_2O is

discussed by *Wang et al.* [2002] and *Taha et al.* [2004], respectively. The precision of SAGE II O_3 is estimated to be ~ 2% [*Borchi and Pommereau*, 2006] and no credible estimates of the precision of H_2O measurements exist. The SAGE II coverage follows a pattern similar to that of HALOE. Geolocation information, including line-of-sight (LOS) angle, was provided on the measurement grid in separate files.

2.1.5. SAGE III The SAGE III instrument [http://science.hq.nasa.gov/missions/satellite_8.htm] used radiances from several channels in the 570 to 600 nm region to derive O_3 and at several more in the 925 to 960 nm region to derive H_2O; it took measurements from May 2002 through December 2005. The instrument and the retrieval algorithm, as well as O_3 validation, are discussed by *Mauldin et al.* [1985], *McCormick et al.* [2002], and *Wang et al.* [2006]. SAGE III data used here are Version 3. O_3 and H_2O data have a vertical resolution of ~ 1 km. The precision of SAGE III O_3 has not been objectively estimated but should be comparable to SAGE II. The SAGE III coverage from the sun synchronous orbit is confined to mid to high latitudes with sunrise events in the southern hemisphere and sunset events in the north. Geolocation information is included in the SAGE III data files every 10 km; this is interpolated linearly to the 0.5-km data grid.

2.2. Aura MLS Dataset

MLS measures millimeter- and submillimeter-wavelength thermal emission from the limb of Earth's atmosphere. Detailed information on the measurement technique and the MLS instrument on the EOS Aura satellite is given by *Waters et al.* [2006]. The Aura MLS fields-of-view point in the direction of orbital motion and vertically scan the limb in the orbit plane, leading to data coverage from 82°S to 82°N latitude on every orbit. Vertical profiles are measured every 165 km along the suborbital track and have a horizontal resolution of ~ 200–300 km along-track and ~ 3–9 km across-track. Vertical resolution of the Aura MLS data is ~ 3–4 km in the lower and middle stratosphere, depending on the product [*Froidevaux et al.*, 2006; *Livesey et al.*, 2005, available from the MLS web site, http://mls.jpl.nasa.gov].

Numerous species are retrieved from MLS observations; examples using DMPs to compare many of these with the SO datasets are presented here. Further details on these species are given in papers in this issue: *Lambert et al.* [2007] (N_2O and H_2O), *Froidevaux et al.* [2007b], *Jiang et al.* [2007], and references therein (O_3), *Froidevaux et al.* [2007a] (HCl), *Santee et al.* [2007b] (HNO_3), *Pumphrey et al.* [2007] (CO), and *Schwartz et al.* [2007] (temperature). These papers validate version 2.2 (v2.2) MLS data and discuss changes from

version 1.5 (v1.5); initial validation comparisons of v1.5 MLS data are given by *Froidevaux et al.* [2006] and *Barrett et al.* [2006]. Reprocessing with MLS v2.2 is ongoing and will take over a year to complete; a small subset of the MLS data spaced throughout the mission have been reprocessed in v2.2. Several of the comparisons shown here focus on reprocessed periods, but we also show some comparisons with v1.5 for examples involving timeseries for which v2.2 data are not yet available.

2.3. Meteorological Analyses

DMPs are currently calculated from the Met Office (MetO) dataset for each of the instruments, from the NASA Global Modeling and Assimilation Office's (GMAO) Goddard Earth Observing System (GEOS) datasets (4 and/or 5) for MLS and ACE, and from the NCEP/CPC (National Centers for Environmental Prediction/Climate Prediction Center) analyses for SAGE II. A brief description of these datasets follows; further information is given by *Manney et al.* [2005b, and references therein], which also provide comparisons between these and other meteorological datasets. *Pawson et al.* [2007, this issue] also show some comparisons for the Aura mission time period of GEOS-4 and 5 with other analyses.

The MetO data through 12 March 2006 are from the stratosphere-troposphere (STT) data assimilation system first developed for the Upper Atmosphere Research Satellite (UARS) project [*Swinbank and O'Neill*, 1994], and have been produced since October 1991. The assimilation used an analysis-correction scheme as described by *Lorenc et al.* [1991] until late 2000, when a three-dimensional variational (3D-Var) scheme was implemented [*Lorenc et al.*, 2000]. In late 2003, a new dynamical core [*Davies et al.*, 2005] was implemented in the assimilation system [*Swinbank et al.*, 2002, 2004]. The MetO-STT data (three-dimensional winds, temperature, and geopotential height) are supplied once-daily at 12UT on a 2.5° latitude by 3.75° longitude grid, and at UARS pressure levels (6 levels per decade in pressure) between 1000 and 0.3 hPa (0.1 hPa after late 2003). After 12 March 2006, the stratospheric analyses are provided from the same numerical weather prediction (NWP) model system as operational forecasts from the Met Office [D. Walters, et al., "Enhancing Vertical and Horizontal Resolution in the Met Office Global NWP (Unified) Model, in preparation]; the same fields are provided, but on a 0.375° latitude by 0.5625° longitude grid, at 27 levels from 1000 to 0.4 hPa. When there is a need to distinguish, the recent MetO analyses are referred to as MetO-NWP and the original ones developed for UARS as MetO-STT. DMPs are calculated for all instruments from the MetO data.

The GEOS-4 analyses are described by *Bloom et al.*

[2005]; a Physical Space Statistical Analysis Scheme is used. The GEOS-4 data used here are provided on 55 hybrid (σ/pressure) model levels from the surface to 0.01 hPa. The horizontal grid is 1.0° latitude by 1.25° longitude. six-hourly average fields are provided centered at 0, 6, 12 and 18 UT. Besides the standard meteorological variables, GEOS-4 products include an extensive set of fields from the model and assimilation system, including PV calculated internally in the model. DMPs for ACE and for MLS v1.5 data are calculated from GEOS-4.

GEOS-5 analyses [*Reinecker et al.*, 2007] have been produced for the full period of the Aura mission, and will eventually replace GEOS-4. GEOS-5 uses the Gridpoint Statistical Analysis method of *Wu et al.* [2002], a 3D-Var system, with a six-hour analyses window. Analyses are produced for surface pressure, temperature, winds, moisture and ozone. Along with operational meteorological products, the AIRS data stream from EOS-Aqua was assimilated, as described in *Stajner et al.* [2007]. The interface between the observations and the GCM is performed using the incremental analysis update (IAU) approach [*Bloom et al.*, 1996], which avoids shocking the model, thus producing smoother analyses. An evaluation of some aspects of GEOS-5 relevant to the Aura mission is presented in *Pawson et al.* [2007, this issue]. GEOS-5 analyses are provided on 72 model levels from the surface to 0.01 hPa, and a 0.5° latitude by 2/3° longitude grid. DMPs for ACE and for MLS v2.2 data are calculated from GEOS-5.

NCEP/CPC analyses (used for SAGE II DMPs) are from an objective analysis at levels above 10 hPa (above 100 hPa prior to April 2001) [*Finger et al.*, 1965, 1993; *Gelman et al.*, 1986, 1994]; these analyses have been available since June 1979. Analyses at and below 100 hPa are from the tropospheric analysis and forecast cycle [e.g., *Derber and Wu*, 1998; *McNally et al.*, 2000]. The NCEP data are provided once a day at 12UT on a 65×65 point polar stereographic grid for each hemisphere; the fields used here are interpolated to a 2.5°×5° latitude/longitude grid. Only temperature and geopotential height are provided in the stratosphere, so horizontal winds are calculated from the NCEP geopotential heights using a form of the primitive equations that neglects the vertical advection and time tendency terms [*Randel*, 1987; *Newman et al.*, 1989].

3. DMP Field Description

Table 1 lists the DMPs calculated for the SO instruments; these DMPs are produced on the vertical grids used for the SO instruments' data. Table 2 lists the DMPs provided for the MLS instrument. MLS records over 100 times more profiles per day than the SO instruments, so calculat-

Table 1. Derived Meteorological Product (DMP) Fields and Units for Solar Occultation Instruments

Field	Units	Description
Geolocation (from Instrument Geometry)		
Alt	km	(2D[1]) Altitudes
Lat	deg	(2D) Latitudes as a function of Altitude
Lon	deg	(2D) Longitudes as a function of Altitude
Sun Dir[2]	deg cw from N	(2D) Line-of-Sight angle (LOS)
Interpolated from Meteorological Data		
Temperature	K	(2D) Temperature from meteorological data
Geop Hgt	m	(2D) Geopotential Height
Zonal Wind	m/s	(2D) Zonal Wind
Merid Wind	m/s	(2D) Meridional Wind
Calculated from Meteorological Data		
θ	K	(2D) Potential Temperature from met data
PV[3]	$10^{-4}\,\mathrm{K\,m^2\,kg^{-1}\,s^{-1}}$	(2D) Potential Vorticity
Scaled PV	$10^{-4}\,\mathrm{s^{-1}}$	(2D) Scaled PV, in "vorticity units"[4]
EqL	deg	(2D) Equivalent Latitude
Hor PV Grad	–	(2D) Normalized horizontal PV gradient
Hor T Grad	K/km	(2D) Horizontal temperature gradient
LOS T Grad[2]	K/km	(2D) Temperature gradient along LOS
LOS PV Grad[2]	$(10^{-4}\,\mathrm{K\,m^2\,kg^{-1}\,s^{-1}})/\mathrm{km}$	(2D) PV gradient along LOS
EqL - VEC	deg	(2D) Distance (EqL) from vortex edge center
EqL - VEI	deg	(2D) Distance (EqL) from inner vortex edge
EqL - VEO	deg	(2D) Distance (EqL) from outer vortex edge
Dyn Tropopause	km	(1D[1]) Dynamical tropopause altitude[5]
TG Tropopause	km	(1D) WMO tropopause altitude

[1] 2D indicates profile information, 1D a single value for each occultation
[2] Not Available for ACE or HALOE DMPs
[3] Interpolated directly from provided dataset for DMPs derived from GEOS-4
[4] *Dunkerton and Delisi* [1986]; *Manney et al.* [1994b]
[5] 3.5 PVU joined to 380 K θ in tropics, see text

ing the DMPs is computationally intensive. To make the calculations feasible, and since the MLS positions are not altitude-dependent, MLS DMPs are calculated and output on standard θ or pressure levels, allowing the calculations to be done in advance on the gridded meteorological analysis fields once for each analysis time, and then interpolated to the MLS times and positions. File formats and access to the DMPs are described in the Appendix; the DMP calculations are described in more detail below.

3.1. Description of Calculations and Interpolations

Interpolation of fields provided in the meteorological analyses (horizontal winds, temperature, geopotential height, PV from GEOS-4 and GEOS-5 analyses) is done linearly in time (between six-hourly fields for the GEOS analyses, daily fields for the MetO analyses) and bi-linearly in latitude and longitude. Vertical interpolations are linear in $\log(\theta)$ for PV or $\log(\text{pressure})$ for the other products. EqL is calculated on isentropic surfaces and interpolated linearly in $\log(\theta)$; for the high resolution MetO-NWP and GEOS products, the computationally intensive EqL calculation is done once and EqL saved on standard isentropic surfaces; these files are read in and interpolated as for PV. For the MetO and NCEP DMPs, PV is calculated as described by *Manney et al.* [1996b], based on the algorithm of *Newman et al.* [1989]; PV is provided from the assimilation model in the GEOS datasets, and this is used in the DMP files, as it is more fully consistent with the analyzed fields than an offline calculation. Scaled PV (sPV) is in "vorticity units" [10^{-4} s^{-1}, *Dunkerton and Delisi*, 1986; *Manney et al.*, 1994b], giving a similar range of values at levels throughout the stratosphere.

Horizontal PV gradients for the SO instruments are calculated using PV interpolated to the isentropic level of each measurement in the profile, and on the standard θ surfaces for MLS. The PV gradients provided in the DMP files are normalized to the hemispheric average on isentropic surfaces; the calculation is also strongly dependent on the resolution of the meteorological analysis used; thus, the magnitudes of gradients calculated from different meteorological analyses are not directly comparable. Horizontal temperature gradients for the SO instruments are calculated on the pressure level of each measurement. LOS PV and temperature gradients are provided for several of the SO instruments for which the LOS angle information is available. These are potentially useful for validation and data quality studies in assessing the homogeneity of atmospheric conditions along the LOS. As with the horizontal gradients, the LOS PV (temperature) gradients are calculated on the θ (pressure) level of each measurement.

The vortex edge "center" position is defined as the EqL of the maximum of the windspeed times the PV gradient. This is very similar, but not identical, to the widely used criterion described by *Nash et al.* [1996]. The "inner" and "outer" vortex edges are EqL on vortex and extravortex sides, respectively, where that vortex definition function changes curvature, as described for PV gradient by *Nash et al.* [1996]. The vortex is considered to be undefined if θ < 345 K, or if any of the following apply: The EqL value at the vortex edge center is greater than 80° (vortex too small, e.g., *Manney et al.* [1994a]), the windspeed is less than 15.2 m/s (polar night jet is too weak, e.g., *Nash et al.* [1996]), or the normalized PV gradient is less than 1.1 (PV gradient is not significantly above average). Figure 1 shows the windspeed, PV gradient, and calculated vortex edge center position from MLS GEOS-4 DMPs during northern hemisphere (NH) winter and spring (SH winter cases, not shown, are less ambiguous since vortex is strong and simply-defined). Every day is included in the monthly averages for PV gradient and wind speed, but only those days on which a vortex edge is defined for the position relative to the vortex edge; thus, in some cases (e.g., SH lower stratosphere in March, when vortex is just starting to develop and does so substantially over the month) there is a vortex edge defined when the plotted PV gradients and windspeeds do not show an obvious transport barrier. The inclusion of windspeed in the definition reduces the likelihood of spurious maxima in the PV gradient at high EqL being identified as the vortex edge, and the use of the combined function provides a means for choosing which of double peaks in windspeed and PV gradient [common in fall, e.g., *Manney et al.*, 2002] are selected. Note that at the lowest levels in January, the top of the upper tropospheric subtropical jet is mis-identified as the vortex edge; this is a common occurrence, but setting the θ limit for the vortex to be defined higher would eliminate much of the SH subvortex region in winter and spring. In the upper stratosphere, and near the stratopause, the jet/PV gradient structure is much more complex, and thus mis-identification (e.g., January in SH) is common; in fact, there is often not a single most appropriate definition of the vortex edge here. Part of the ambiguity is in the PV field, because of the decreased static stability in the region surrounding the stratopause; far above the cold pool, this layer is often nearly isothermal.

Automated vortex edge definition is most robust under conditions for which the vortex is well, and simply, defined, i.e., when there is a single region of strong PV gradients associated with the polar night jet. This is the case in the middle to lower stratosphere during SH winter and many NH winters; in these cases the definition used here agrees closely with that of *Nash et al.* [1996] and with other methods of determining the vortex edge (including simply using a representative sPV contour). In the upper stratosphere, vortex-edge location is more ambiguous and dependent on the spe-

Table 2. Derived Meteorological Product (DMP) Fields for MLS

Field	Units	Description
On Standard Pressure Surfaces		
Pressure	hPa	Standard Pressure Level Values
θ	K	Potential Temperature from met data
Geop Hgt	m	Geopotential Height
On Standard Potential Temperature Surfaces		
θ	K	Standard θ level values
Pressure	hPa	Pressure on θ surfaces
Zonal Wind	m/s	Zonal Wind
Merid Wind	m/s	Meridional Wind
PV	$10^{-4}\,\mathrm{K\,m^2\,kg^{-1}\,s^{-1}}$	Potential Vorticity
EqL	deg	Equivalent Latitude
Hor PV Grad	–	Normalized horizontal PV gradient
EqL - VEC	deg	Distance (EqL) from vortex edge center
EqL - VEI	deg	Distance (EqL) from inner vortex edge
EqL - VEO	deg	Distance (EqL) from outer vortex edge
Single-Level Fields		
Latitude	deg	MLS Level 2 reported latitude
Longitude	deg	MLS Level 2 reported longitude
Dyn Tropopause	hPa	Dynamical tropopause pressure
TG Tropopause	hPa	WMO tropopause pressure

cific method of definition. During spring and fall the automated determination also can become problematic. Figure 2 shows the vortex edge as a function of time, versus sPV and ACE CH_4, for December through March 2005, in the upper and lower stratosphere; in mid-March 2005, the vortex began to break up in a major final warming [e.g., *Manney et al.*, 2006]. In the lower stratosphere, the vortex edge is marked by a very well defined region in sPV and CH_4 (and other trace gases and dynamical markers such as windspeed, PV gradient and EqL, not shown) in January through late March, becoming slightly less distinct only after mid-March during the final warming. Behavior in the middle stratosphere (not shown) is similar, with more indication of mixing in CH_4 as the vortex became more variable in late February. In the upper stratosphere, the region of the vortex edge is much less defined throughout the winter because of its complex structure. Thus, while the automated vortex edge criterion (and any similar criteria) is robust for studies of the winter middle and lower stratosphere during relatively quiescent conditions, for studies involving the upper stratosphere and/or fall and spring when the vortex is more variable, due caution should be used in applying such automated definitions, and their appropriateness should be checked against the physical conditions. Note further that the conditions under which this, or any other, automated vortex edge definition is robust are exactly those under which any reasonable definition of the vortex edge (including, e.g., a specific sPV contour) will provide a comparable value.

The WMO (temperature gradient) tropopause is defined as the lowest altitude where the temperature lapse rate drops below 2 K/km and remains below that for at least 2 km. The WMO tropopause is calculated using the algorithm of *Reichler et al.* [2003]. For the SO instruments, it is calculated from the meteorological analyses' temperatures after they have been interpolated to the SO instrument's measurement location and vertical grid; for MLS it is calculated before interpolation on the native grid of the meteorological analysis and interpolated to the MLS times/positions. The "dynamical" tropopause is defined by the 3.5×10^{-6} PV contour in the extratropics, joined to the 380 K isentropic surface in the tropics or subtropics where that PV contour rises above this level. The 3.5×10^{-6} PV definition is consistent with the value found to be appropriate for the extratropics by *Highwood and Berrisford* [2000] and *Schoeberl* [2004]. Tropopause altitude is saved for the SO instruments, and pressure for MLS, according to the native vertical grid of the data. Figure 3 shows the WMO and dynamical tropopause altitude for MLS and the five SO instruments during January 2005. The WMO and dynamical tropopause calculations agree quite well in the summer hemisphere (SH) through midlatitudes in the winter hemisphere (NH); as noted previously [*Highwood and Berrisford*, 2000, and references therein], there is often a deep, nearly isothermal layer in the polar winter, and thus the WMO tropopause is often not very well defined. At the latitudes covered by the SO instruments, the range of tropopause val-

ues sampled by them is typically similar to that sampled by MLS; fewer values from the SO instruments in the low end of the range may simply reflect inaccuracy in the conversion of the MLS tropopause location from pressure to altitude. The SO data also show fewer high values at the WMO tropical tropopause, which may be related to the finer vertical grid used to locate the tropopause for the SO instruments.

3.2. Sampling Issues

The DMPs help us to explore the effects of sampling and coverage on a variety of comparisons and analyses of the satellite data by providing versions of the same fields as sampled by different instruments.

Even with the relatively dense coverage of MLS, the sampling can have a substantial effect on how we view the atmosphere. Figure 4 shows PV from the 1x1.25° GEOS-4 analyses in the lower and upper stratosphere, and maps of the same fields gridded from the MLS GEOS-4 DMPs. (MLS fields are mapped on a 2x5° grid using a weighted average of all the points in a day within a specified distance of the gridpoints, as is commonly done for "quick-look" maps.) The day shown is a case where the MLS sampling captures some small scale features quite well, e.g., the intrusion into the vortex near 30°E at 490 K, and the very narrow double filament drawn off the vortex near 120–180°E, 30°N at 1700 K. However, much of the small-scale structure inside the vortex at 1700 K is either distorted or not apparent in the MLS DMP fields, and other small-scale features are smeared out (e.g., the small high/low PV dipole near 310°E, 30°N at 490 K). When comparing features in PV with MLS trace gas observations, it is often helpful in assessing agreement to view the PV fields as sampled by MLS. With the sparse coverage of the SO instruments, sampling effects are always an important consideration. Figure 5 shows the latitude sampled by each of the five SO instruments used here as a function of EqL in the lower stratosphere during the 2004-2005 NH winter period that will be the focus of time-series comparisons shown here, along with the sPV as sampled by those instruments. As seen in Figure 2, and apparent in the location of strong gradients, the vortex edge is near 1.3-1.5×10^{-4} s^{-1} at this level. HALOE and SAGE II sampled very little vortex air during the winter. SAGE II coverage moves into the vortex in late February, largely because of the increasing variability in vortex shape and position [e.g., *Manney et al.*, 2006], but note that, although its measurements in the latter half of March reached the highest EqLs, they were taken at much lower geographical latitudes than those of the other instruments measuring inside the vortex at this time ($\sim$55-65° as opposed to $\sim$68-85°). Throughout the winter, the three instruments that measured primarily at high latitudes (ACE, POAM III, SAGE III) also covered high EqLs by measuring

at quite different latitudes at a given time. While this should not be a large factor in comparing them for species that follow the vortex closely (e.g., N_2O), it can be significant for species that may be affected by processes that do not align as well with the vortex (e.g., O_3, temperature), as will be seen in section 4.

Figure 5 also shows a wide variation in density and completeness of coverage of the vortex. This may have a strong effect on our perception of vortex-averaged values when looking at results from different instruments. The extreme example is when comparing MLS (which has nearly complete coverage of the vortex with dense sampling every day) with the SO instruments. Figure 6 shows the average latitude of all measurements inside the vortex (defined by the 1.4×10^{-4} s^{-1} sPV contour, c.f., Figure 2) during the NH 2004-2005 fall and winter, from MLS and ACE measurements. As expected, MLS average latitudes are typically from $\sim$65° to $\sim$72°N during the winter (except at lowest levels where vortex is smaller), decreasing dramatically during the vortex breakup starting in early March as the vortex shrinks and its remnants move away from the pole. In contrast, the latitude from the SO instruments is determined almost entirely by their measurement patterns, as seen for ACE. In section 4, we show examples of vortex-averaged trace gas comparisons between MLS and SO instruments, using the full MLS sampling and a sampling coincident with that from an SO instrument to demonstrate how this may affect intercomparison results.

4. Comparisons of MLS with Solar Occultation Data Using DMPs

In the following, we show comparisons of several MLS species with SO instrument data using the DMPs to assist in comparing measurements in the same air masses. The main types of displays are EqL/θ vertical sections, EqL/time series, and vortex averages. The EqL/θ plots are produced by taking weighted averages around each gridpoint in EqL, θ and uncertainty (as provided in each instrument's data files) as described by *Manney et al.* [1999, 2001]; a Gaussian weighting function is used. The EqL grid spacing is 5°, with all points out to four half-widths included to maximize coverage for sparse SO instruments; thus, many MLS points are included in the average for each gridpoint. The θ grid is equally spaced in ln(θ), with $\sim$0.09 spacing, corresponding to an $\sim$3-km grid, comparable to the resolution of many of the instruments, and generally coarser than the data grids; two half-widths are included in θ. EqL/time plots are produced in the same way, but with gridding in time instead of θ. Time gridpoints are 12 UT each day. The SO instruments have a 5° latitude half-width and 3-day time

half-width, with 3 half-widths included for each. For the qualitative time-series comparisons shown here, we have retained 2.5° latitude, 1.5 day time half-widths for MLS, with three half-widths included in each direction. The philosophy of the uncertainty weighting is similar to that of *Manney et al.* [1999]: A relatively narrow half-width is chosen, with many half-widths included, so that only points with extremely large uncertainties are excluded but the most precise data are given much higher weight.

For vortex averages, the vortex edge is defined by the 1.4×10^{-4} s^{-1} sPV contour; very similar results are obtained using the EqL from the vortex edge center. For both SO and MLS, the measurements are interpolated linearly in $\ln(\theta)$ to the plot grid, and all points in the vortex on a day are binned and averaged. For averages of MLS measurements coincident with SO observations, the criteria are $\pm 1°$ latitude, $\pm 8°$ longitude, and 12 hours.

Timeseries plots (EqL/time and vortex averages) are done using MLS v1.5 data, to show consistency of time evolution and specific features; comparisons that involve only ACE and MLS use GEOS-4 DMPs, others use MetO DMPs. EqL/θ plots are done using 6- to 8-day periods for which all MLS data have been reprocessed in v2.2 for more quantitative comparisons; these periods include 25–31 January 2005, and 10–16 March 2005. EqL/θ plots use GEOS-5 DMPs for comparisons with ACE, and MetO for all others; where the satellite data are recommended for use at those levels, MLS/ACE comparisons are shown to the higher altitudes allowed by the GEOS-5 DMPs.

4.1. Ozone

Stratospheric O$_3$ monitoring is one of the primary focuses of the Aura MLS experiment. O$_3$ measurements are available from MLS and all of the SO instruments considered here. *Froidevaux et al.* [2007b, this issue] and *Jiang et al.* [2007, this issue] discuss quality and validation of v2.2 MLS O$_3$, as well as differences between v1.5 and v2.2.

Figure 7 shows a comparison of the time evolution of O$_3$, using MLS v1.5 data, in the lower stratosphere during the 2004-2005 NH winter. Differences between v1.5 and v2.2 O$_3$ at this level are small: V2.2 is, on average, $\sim$2–4% lower in the lower stratosphere [*Froidevaux et al.*, 2007b, this issue]. 2004-2005 was arguably the winter with the largest lower stratospheric chemical O$_3$ loss of any NH winter [*WMO*, 2007, and references therein]. The morphology of O$_3$ was also complex, being highest near the vortex edge even before chemical loss began; this complicates separation of dynamical and chemical effects and makes assessment of O$_3$ loss more problematic [e.g., *Manney et al.*, 2006]. It is clear that the O$_3$ evolution in the vortex and along its edge agrees quite well, both quantitatively and qualitatively,

between the four instruments, MLS, ACE, POAM III, and SAGE III, with good coverage of the vortex. SAGE II values along the vortex edge and in late March also agree quite well. POAM III and SAGE III show slightly higher values in 40–60°EqL than MLS, SAGE II and HALOE; this may be a sampling effect, as the POAM III and SAGE III measurements are all taken at higher latitudes where high O$_3$ values are not completely aligned with the vortex [see, e.g., maps in *Manney et al.*, 2006]. ACE vortex interior values are slightly higher overall than those from the other instruments, but with a very similar amount of O$_3$ decrease between January and March to that of the other instruments. Examination of late-January/mid-March differences as a function of EqL and θ (Not shown) from SO instruments and MLS v2.2 data indicate very similar amounts of decrease in the lower stratospheric vortex (a signature of chemical loss) for each of the instruments, $\sim$0.9 ppmv in MLS, POAM III and SAGE III and $\sim$1.1 ppmv in ACE, with maximum changes very closely colocated near 70°EqL and 490 K. Detailed calculations [*Singleton et al.*, 2007] for this winter showed very good agreement in O$_3$ loss estimated from these instruments, especially when MLS v1.5 data were sampled similarly to the SO instruments.

Figure 8 shows vortex averages of MLS and ACE O$_3$, along with a vortex average of the MLS points that are coincident with ACE. This clearly demonstrates some sampling effects. In the lower stratosphere, below $\sim$600 K, MLS and ACE vortex averages agree very well; these are levels where, in absence of heterogeneous chemistry, the lifetime of O$_3$ is very long, and when chemical loss does occur, the patterns are generally aligned with the vortex. In the middle and upper stratosphere, in contrast, the full MLS average shows considerably lower values than ACE, and significant differences in time evolution, especially in the episodes of higher vortex O$_3$ (associated with periods of increased wave activity). By averaging only those points coincident with ACE measurements, most of the qualitative differences in time evolution are eliminated, and the MLS values at the O$_3$ maximum are increased, lessening the difference from ACE. The coincident MLS vortex average above $\sim$800 K is typically $\sim$0.3–0.6 ppmv less than that for ACE, generally consistent with the results of *Froidevaux et al.* [2006] for hemispheric averages of MLS v1.5 and ACE v2.1 data.

Figures 9 and 10 compare v2.2 MLS O$_3$ with each of the SO instruments during March 2005. First, Figure 9 shows MLS O$_3$ mapped in EqL/θ using the GEOS-5 and the MetO DMPs, and the difference between them; this demonstrates that the differences in gridding from using different DMPs are small compared to differences seen below between instruments. ACE comparisons in Figure 10 use GEOS-5 DMPs and extend to higher levels; other compar-

isons use MetO DMPs for MLS as well as SO instruments. Figure 10 shows very good agreement between all instruments in the lower stratosphere and around the tropopause; differences are typically less than 0.2 ppmv, and, even at these low O_3 values, less than ~5%. The exceptions are high biases with respect to HALOE and SAGE II in the NH tropics and mid-EqLs at the lowest levels, and low biases with respect to ACE at the same levels near ±40°EqL, at the edges of its coverage. In the middle to upper stratosphere (~900–1600 K) near 40–60°EqL, MLS is higher than ACE, POAM III and SAGE III (high-latitude-sampling instruments) and lower than SAGE II and HALOE (low-latitude-sampling instruments). This is the region where "low-ozone pockets" (LOPs) [*Manney et al.*, 1995b; *Harvey et al.*, 2004] are common: High O_3 from low latitudes is drawn into and trapped in the anticyclone for many days. When thus confined at high latitudes, O_3 relaxes chemically toward the lower equilibrium values for these latitudes (whereas air outside the anticyclones is continually being mixed with higher-O_3 air from low latitudes). The pattern seen in MLS data, with highest values apparently excluded from this EqL band, is characteristic of the morphology seen when a LOP is present [e.g., *Manney et al.*, 1999, 2001]. LOPs were observed continuously from early December 2004 through late March 2005 [V. L. Harvey et al., "Low-ozone pocket definition using EOS-MLS observations", in preparation, 2007, hereinafter *Harvey et al., in prep.*]; these LOPs were sampled by MLS and all SO instruments examined here. Figure 11 shows a time-series at 850 K for MLS v1.5, POAM III and HALOE; MLS v1.5 and v2.2 typically differ by <2% in the middle stratosphere, [*Froidevaux et al.*, 2007b, this issue]. HALOE provided excellent observations of LOPs in January and February (green region outside vortex). POAM III sampling of LOPs was best in March when the anticyclone was at very high latitudes. The "pulses" seen in multiple extra-vortex ozone minima (especially in MLS where sampling issues are minimal) are associated with anticyclone merger events [*Harvey, et al., in prep.*]. None of the SO instruments sample the LOPs and anticyclone region as fully as MLS. Conversely, there are cases where an SO instrument samples a tongue of very high O_3 drawn up between the vortex and anticyclone that is missed by MLS [it Harvey, et al., in prep.]. EqL/θ comparisons like those in Figure 10 constructed using only MLS observations coincident with the SO instruments (not shown) reduce the differences in the middle stratosphere to less than ~0.4 ppmv, and in some cases change the sign (e.g., MLS is slightly lower than ACE in this region), conclusively demonstrating that these differences result from the interplay of sampling, transport and chemistry in this region. These differences are of a similar character to those found

by *Manney et al.* [2001], and vary with the time period examined, depending on the presence and sampling of LOPs and low-latitude filaments; similar patterns are seen in EqL/θ comparisons during the 2005 SH late winter (not shown).

In the upper stratosphere (and lower mesosphere for ACE), Figure 10 shows MLS O_3 to be low with respect to ACE and SAGE III; this difference is global and persistent across the time periods examined. Similar differences were seen by *Froidevaux et al.* [2006] with respect to ACE; *Walker et al.* [2005] also noted that ACE v1.0 O_3 was high with respect to other instruments from about 40 to at least 60 km, and this difference persists in v2.2 ACE data. *Froidevaux et al.* [2007b, this issue] show a few percent increase in v2.2 over v1.5 in the upper stratosphere, with a continuing low bias (by ~5–10%) with respect to v2.2 ACE data in v2.2 MLS data. The high bias of MLS with respect to ACE in the lower mesosphere above ~3000 K is also persistent across the periods examined.

Figure 12 shows O_3 at the tropopause from MLS v2.2 data and each of the SO instruments for 18-day periods in January–February and September 2005. Since O_3 gradients across the tropopause are extremely strong [in fact, O_3 is sometimes used to define the tropopause, e.g., *Bethan et al.*, 1996], this is a very sensitive comparison; also, in this region of very low O_3 and increasing possibility of clouds, the retrievals are difficult. Overall, the values agree remarkably well, especially considering that measurements at the same latitude from different instruments may have been taken several days apart. In January, all instruments show cases of negative O_3 values, indicating difficulties in retrieving such low O_3 values, but most of the values are ~0.1 to 0.4 ppmv at the dynamical tropopause, consistent with previous estimates [e.g. *Bethan et al.*, 1996; *Pan et al.*, 1997]. The MLS average at the dynamical tropopause, near 0.15 ppmv, agrees quite well with the center of the distributions for ACE and SAGE III, and is slightly higher than HALOE and POAM III. Ozone varies more at the WMO tropopause, and shows a very large scatter in the winter polar regions, where that definition of the tropopause is most ambiguous (Figure 3); MLS, ACE, and SAGE III all show large (near 2.0 ppmv) values here in January/February, when the temperatures and tropopause height were highly variable [e.g. *Schoeberl et al.*, 2006] and the WMO definition can be ambiguous; a similar plot for March 2005 (not shown), when the WMO tropopause is better defined, shows much lower, more typical, values in the Arctic. A very similar pattern is seen in the Antarctic winter, but with less scatter in the O_3 values for all instruments, likely due to more symmetric conditions in the SH winter resulting in more uniform sampling.

The preceding discussion of O_3 indicates overall very good agreement between MLS and all of the SO instruments

studied, but highlights many of the sampling issues that are important in interpretation of sparse measurements. Mapping in EqL is very valuable in scientific studies with SO data, allowing examination of the full range of conditions sampled and averaging of air from similar air masses. But, particularly with chemically active species such as O_3, great care must be taken to understand how the sampling may affect the interpretation of the results. Comparisons such as those shown above not only help assess the consistency of MLS and SO data, but also can assist in understanding and interpreting sampling effects to get the maximum information from the sparse SO datasets for scientific studies and for validation comparisons with other sparse measurements.

4.2. Long-lived Tracers

Three species measured by MLS that are commonly used as tracers of transport are N_2O (in the lower and middle stratosphere), H_2O (throughout the stratosphere and into the mesosphere) and CO (mid-upper stratosphere and mesosphere; also upper troposphere and lowermost stratosphere). Figure 13 shows vortex averages in the 2004-2005 NH fall and winter of these three species, from ACE and MLS. The vertical range for CO and H_2O extends just across the stratopause; N_2O is shown only to the upper stratosphere. In general, the strong descent from the mesosphere through the middle stratosphere is represented very well in both datasets in CO and H_2O, with the ACE sampling capturing the extent and timing of it. Variations in the lower stratosphere (highlighted in N_2O) are not quite as fully represented in ACE, but after about 15 January, the magnitude of decreases and then increases in N_2O is correctly estimated by ACE. During early October through early January (across the gap in ACE data), mixing into the vortex resulting from strong wave activity led to increases (decreases) in vortex-averaged N_2O (H_2O) in the lower through middle stratosphere. When MLS is sampled like ACE, however, a significant overestimate of these increases results, since ACE sampled near the edge of the vortex at this time, where N_2O (H_2O) is higher (lower) and mixing in of outside air is greater. "Vortex-averages" such as this from SO instruments are often used to estimate descent rates for polar processing studies [e.g., *Nassar et al.*, 2005] – situations such as this could lead to a substantial overestimate of descent from ACE measurements after the period of strong mixing.

Comparing ACE with coincident MLS measurements shows very good quantitative agreement in CO and H_2O in most regions, but slightly lower MLS H_2O near the stratopause. N_2O shows excellent qualitative agreement in time evolution, but a slight overall low bias of MLS with respect to ACE, as was noted for NH means of coincident profiles by *Froidevaux et al.* [2006]. V2.2 MLS N_2O is on

average about 10% higher than v1.5 between 46 and 2 hPa [*Lambert et al.*, 2007, this issue], which would reduce the bias seen here.

4.2.1. N_2O Figure 14 shows times series as a function of EqL at 490 and 850 K of MLS v1.5 and ACE N_2O. Very good qualitative agreement is seen at both levels, and quantitative agreement at 850 K. At 490 K, MLS is considerably lower inside the polar vortex and slightly higher outside, with stronger gradients across the vortex edge. Sampling effects could be a factor in the differences outside the vortex, since ACE is sampling primarily at high latitudes, where the ambient N_2O is lower, and may miss sampling lower latitude air that is not precisely correlated with the PV fields used in the EqL mapping. The low MLS bias in the vortex will be reduced somewhat in v2.2 [*Lambert et al.*, 2007, this issue], and sampling may contribute to it as well (but see below) because the sparse sampling of ACE may miss extreme values that are represented in the MLS N_2O fields; however, a low bias in the vortex with respect to ACE appears to be a persistent feature in both versions of MLS data, and is consistent with the results of *Lambert et al.* [2007, this issue].

EqL/θ sections comparing MLS v2.2 and ACE data are shown in Figure 15 for the NH in March; similar patterns of difference appear in plots for the SH winter period examined (not shown). These show the persistent low bias of MLS in the polar vortex, and in the summer polar lower stratosphere. Similar plots using only the MLS data coincident with ACE (not shown) have only slightly smaller biases in the lower stratosphere, indicating that sampling differences are not the primary factor producing this pattern. *Lambert et al.* [2007, this issue] also show a low bias in this region in hemispheric averages of differences between MLS and ACE coincident profiles. Elsewhere, localized differences are up to $\sim$15 ppbv, but most areas are within $\sim$5 ppbv, with ACE slightly lower than MLS.

4.2.2. H_2O The time evolution of v1.5 MLS H_2O is compared to ACE in Figure 16 in the lower stratosphere. Vortex H_2O values show very good agreement, but, once again, gradients across the vortex edge are weaker in ACE, leading to generally higher midlatitude ACE H_2O. The consistency of this with the patterns seen in N_2O (Figure 14) suggests that the ACE sampling is the primary factor in this behavior. In contrast, ACE and MLS H_2O agree very well inside the vortex, suggesting that the low bias of MLS N_2O with respect to ACE discussed above and seen in Figure 14 reflects a real difference between the fields being compared. In the middle stratosphere (not shown), MLS and ACE H_2O agree well quantitatively throughout the NH winter; in the upper stratosphere (not shown), time evolution is similar in in ACE and MLS, but ACE has slightly higher overall values. POAM III H_2O (not shown) is noisier and displays

some artifacts; nevertheless, similar time evolution is apparent, but with values biased high with respect to MLS and ACE at all levels.

Figure 17 shows EqL/θ comparisons of MLS v2.2 H_2O with ACE and HALOE during March 2005. MLS and ACE agree extremely well throughout the range, with differences typically under 0.2 ppmv (less than 5%) and maximum localized differences up to 15%. MLS is higher than HALOE by ~0.2–1.0 ppmv (~5–25%) throughout the range shown. SAGE II and POAM III H_2O fields for this period (not shown) are somewhat noisy, but similar comparisons with them show SAGE II to be ~5–15% lower than MLS between 500 and 1600 K, and POAM III to be ~5–15% higher than MLS between 400 and 1600 K. Each of these biases is consistent with hemispheric biases with respect to v1.5 H_2O data in *Froidevaux et al.* [2006]; *Lambert et al.* [2007, this issue] show little overall bias between v1.5 and v2.2 H_2O in the stratosphere.

4.2.3. CO   The chemical lifetime of CO varies from a few weeks to many months, making it a useful tracer of transport [e.g., *Solomon et al.*, 1985; *Allen et al.*, 1999] in many situations; *Filipiak et al.* [2005] showed initial results for MLS CO, and *Clerbaux et al.* [2005] for ACE CO. As shown in Figure 13, starting in fall very high CO descends from the mesosphere into the winter stratospheric vortex. Figure 18 shows the time evolution of MLS v1.5 and ACE CO in the upper stratosphere. Quantitative agreement between ACE and MLS is good, as is also the case in the middle stratosphere (not shown). The combination of sparse sampling and longer time averaging used in the EqL/time gridding for ACE are the primary factors responsible for the small qualitative differences in short-lived features near the vortex edge in late January and early February. *Froidevaux et al.* [2006] showed little overall bias between ACE and MLS v1.5 CO in the stratosphere, but v1.5 CO often has substantial oscillations in the vertical throughout the stratosphere (reduced in v2.2, *Pumphrey et al.* [2007, this issue]) that may result in biases at individual levels.

Figure 19 shows an EqL/θ comparison of MLS v2.2 and ACE CO for March 2005; similar patterns are seen in January and September (not shown). The MLS CO measurement is noisy, as seen in the variations in mid-EqLs in the upper stratosphere, and v2.2 still shows some remaining vertical oscillations in the stratosphere [*Pumphrey et al.*, 2007, this issue]; because of this, and the extremely large range of CO values, difference plots (not shown) are difficult to interpret. However, qualitative agreement is good throughout the range. Quantitative agreement is best in the Arctic lower mesosphere, above about 2000 K (50 km). A high bias of MLS with respect to ACE in most regions, but low bias from ~600 to 800 K, is consistent with profile comparisons shown

by *Pumphrey et al.* [2007, this issue].

4.3. Other Fields

4.3.1. HNO₃ HNO_3 is critical in both the activation and the deactivation of chlorine, and thus indirectly regulates ozone destruction in the stratosphere [*Solomon*, 1999; *Santee et al.*, 2004, and references therein]. In the lower stratosphere (not shown), time evolution of MLS v1.5 and ACE HNO_3 at a function of EqL agrees quite well, but ACE misses some of the lowest values in the vortex indicative of sequestration in PSCs, as expected for such localized features that are not well-correlated with the vortex. In the middle stratosphere (Figure 20, [MLS data are scaled by 0.7 to correct an ~30% high bias because of a spectroscopy error in v1.5, *Santee et al.*, 2007b, this issue]), qualitative evolution appears generally consistent. The low region that develops inside the vortex edge in late January through mid-February provides an illustrative example of differences related to the sparse ACE sampling. Maps of MLS 850 K HNO_3 during this period (Figure 21) show the evolution of a partial band of low HNO_3 just inside the vortex edge (a similar feature appears in v2.2 HNO_3). ACE observation locations are overlaid, and show that ACE typically measured near the edge of this low HNO_3 region where values were slightly higher, and the times (e.g., 5 February) when it did sample near the lowest values were when that region was farther into the vortex interior (thus, at higher EqL); this pattern, and the three-day time half-width used for the ACE gridding, result in the faint (and distorted toward higher EqL and later time) echo of the feature in the ACE data.

EqL/θ comparisons of MLS v2.2 and ACE HNO_3 in January 2005 (Figure 22), during a period of strong PSC activity [*Jin et al.*, 2006], show good qualitative agreement, including the position and morphology of the primary HNO_3 peak and a secondary peak in the polar winter upper stratosphere (~900-1300 K) that is a common feature of the HNO_3 distribution [e.g., *Orsolini et al.*, 2005]. Quantitative agreement is fairly good in the levels surrounding the peak (~550 to 900 K), with MLS typically up to 1.0 ppbv (~5-20%) lower, consistent with the results of *Santee et al.* [2007b, this issue]. Somewhat larger differences are seen in the mid to low EqL lower stratosphere, below ~500 K, and above ~900 K, with MLS biased low. Similar patterns are apparent in the other periods examined. ACE does not capture the region of low HNO_3 in the NH lower stratospheric vortex indicative of sequestration in PSCs; this is, again, a sampling effect, since the region of PSCs is not aligned with PV contours and is limited enough that it is often missed by the ACE sampling.

4.3.2. HCl   HCl is a primary reservoir species of Cl [e.g., *Solomon*, 1999]. *Froidevaux et al.* [2007a, this issue] discuss detailed validation of MLS v2.2 HCl and changes

from v1.5. EqL/time series evolution of MLS v1.5 and ACE HCl in the lower stratosphere during the very cold 2004-2005 NH winter (not shown), when chlorine was activated for a prolonged period [e.g., *Dufour et al.*, 2005], indicates very good quantitative agreement in the evolution of the region of low HCl associated with chlorine activation, and in other features of the time evolution. Figure 23 shows EqL/θ comparisons of MLS v2.2, ACE, and HALOE HCl in January 2005. Agreement between ACE and MLS is very good, typically better than 5%, everywhere above ~550 K, consistent with *Froidevaux et al.* [2006, 2007a, this issue]. In the region of low HCl in the NH vortex, ACE is higher than MLS by up to ~0.4 ppmv, resulting from ACE sampling not covering the location of minimum values sampled by MLS. HALOE HCl is ~5–25% lower than MLS through most of the range, consistent with *Froidevaux et al.* [2006, 2007a, this issue].

4.3.3. Temperature   The use of vortex centered (i.e., EqL) coordinates is not an obvious choice for temperature from a scientific point of view, since temperature is not, in general, expected to be closely spatially correlated with the vortex [e.g., *Manney et al.*, 1996a, 2003; *Mann et al.*, 2002]. However, we are often interested in temperatures within the vortex, and the comparison between MLS and SO instruments can help us understand how the sparse sampling of the SO instruments may affect studies of processes depending on temperature. Also, the EqL coordinate still provides a method of comparing SO measurements with other datasets over a broader range of conditions than can easily be done with individual coincidences or zonal means. The DMPs also provide a convenient way of comparing the satellite datasets' temperatures to those in the meteorological analyses [e.g., *Pawson et al.*, 2007, this issue].

Figure 24 shows vortex-averaged MLS v1.5 and ACE temperatures, and the average of MLS temperature measurements coincident with ACE locations. In the middle and upper stratosphere, all of these agree quite closely, indicating that not only are ACE and MLS temperatures in good agreement, but also that the ACE sampling is representative of a vortex average. In the lower stratosphere, the full MLS vortex average shows more continuous periods of low temperatures (as ACE sampling moves in and out of cold regions), but higher minimum values (when ACE samples cold regions, the "average" is lower than the average including both cold and warmer regions sampled by MLS). ACE minimum values are slightly lower than the coincident ones for MLS; MLS v1.5 temperatures have a known high bias with respect to meteorological analyses and many correlative datasets [e.g. *Froidevaux et al.*, 2006; *Schwartz et al.*, 2007, this issue] throughout the stratosphere; *Schwartz et al.* [2007, this issue] show that v2.2 MLS data typically have a

smaller, low bias with respect to the same datasets.

Figure 25 compares EqL/θ-mapped MLS and ACE temperatures in September 2005, during the SH late winter. ACE is higher than MLS v2.2 almost everywhere, by a much larger amount than the small bias noted by *Schwartz et al.* [2007, this issue]. During this period, there was strong wave activity throughout the stratosphere, with the vortex distorted and shifted off the pole, and a dipole pattern of low/high temperatures across the vortex edge on the side with the anticyclone (Figure 26). ACE measurements were in the outer part of the vortex, so tended to miss the coldest region and sample near the warmest region on most days during the period, resulting in the apparent large high bias with respect to MLS. This shows how strong a factor sampling is in comparisons of temperature, and demonstrates the care that must be taken in interpreting temperatures in vortex-centered coordinates.

5. Summary and Outlook

Derived meteorological products (DMPs) have been calculated and made available for Aura MLS and the solar occultation (SO) instruments ACE, HALOE, POAM II and III, and SAGE II and III. These products are fields from and calculated from gridded meteorological analyses that are interpolated to the observation locations of the satellite instruments. The DMP fields include θ, horizontal winds, PV, horizontal PV gradients, EqL, geopotential height, vortex edge criteria, and tropopause locations; DMP files for some instruments include additional potentially useful quantities such as temperature gradients and line-of-sight PV and temperature gradients. The DMPs have been calculated from the Met Office stratosphere-troposphere assimilation dataset for all instruments; in addition, DMPs from GEOS-4 and GEOS-5 are available for ACE and MLS (GEOS-4 for MLS v1.5 and GEOS-5 for MLS v2.2), and from NCEP/CPC data for SAGE II. DMPs are not limited to the Aura mission time-period, but have been calculated for the entire mission for each instrument. DMPs are provided (see Appendix) with the hope that other researchers will find them useful both for validation and in science studies combining multiple datasets.

Examples comparing MLS and SO data were used to illustrate sampling issues. Situations where these effects can be important include:

- Comparison of fine-scale transport features (e.g., filaments and intrusions into the vortex) as represented in high-resolution gridded meteorological analyses and in MLS data.

- Studies of O_3 in the middle stratosphere in low ozone

pockets, where the combination of chemical and dynamical processes results in O_3 distributions that are not closely aligned with the vortex.

- O_3 distributions in the lower stratosphere when the morphology of O_3 is complex and chemical loss is taking place.

- Studies using N_2O to estimate descent, where the movement of SO sampling from vortex edge to vortex center over time can result in an overestimate of descent using "vortex averages".

- Localized features, such as PSCs (reflected in depressions in gas-phase HNO_3), that are captured by MLS but not by sparse SO sampling.

- Comparisons during polar winter when temperatures are often not concentric with the vortex, such that sparse SO sampling misses extreme values.

SO data are extremely valuable for understanding the atmosphere and monitoring its long-term changes, because of their high vertical resolution and precision, the availability of long, calibrated datasets, and the potential for detecting many species (e.g., ACE). Even greater value is realized in studies combining SO and other data, such as UARS MLS [e.g. *Manney et al.*, 1999, 2000; *Randel et al.*, 1999] and Aura MLS [*Braathen et al.*, 2006; *Singleton et al.*, 2007, M. L Santee, et al., "A study of stratospheric chlorine partitioning based on new satellite measurements and modeling", submitted to *Journal of Geophysical Research – Atmospheres*]. The spatial sparsity of the SO data makes understanding sampling effects critical; using the DMPs, the sampling limitations have been studied extensively here, to help guide interpretation of the SO data and combination of them with other datasets.

Comparisons of MLS and SO data using the DMPs show good agreement in time evolution of MLS and SO observations in examples from the 2004-2005 Arctic winter; specifically:

- Time evolution and values of O_3 in the lower stratospheric vortex agree well between MLS v1.5 and ACE, HALOE, POAM III, SAGE II and SAGE III, and all instruments show a similar amount of decrease indicative of chemical O_3 loss.

- ACE and MLS v1.5 CO and H_2O provide a similar picture of the descent of mesospheric air into the stratospheric vortex, both in magnitude and timing.

- When sampled similarly, the time evolution of ACE and MLS v1.5 CO, H_2O, N_2O, O_3 and temperature averaged in the vortex agree very well.

- MLS v1.5 N_2O shows excellent qualitative agreement with ACE in EqL/time evolution in the middle and lower stratosphere; a low bias of MLS with respect to ACE in the lower stratosphere is a persistent feature.

- MLS v1.5 and ACE H_2O show excellent agreement in EqL/time evolution in the middle and lower stratosphere; likewise for CO in the middle and upper stratosphere.

- MLS v1.5 HNO_3 (scaled to correct a known bias) agrees well with ACE HNO_3 in EqL/time evolution, with differences explained by sampling effects.

Comparisons of EqL/θ sections of MLS v2.2 and SO data show overall good agreement, including:

- O_3 agrees to within 5% for for most comparisons, except in regions where differences in MLS and SO sampling of low O_3 pockets result in larger discrepancies; ACE data in the upper stratosphere and lower mesosphere are slightly low with respect to MLS and other instruments.

- MLS v2.2 N_2O shows a persistent low bias with respect to ACE in the polar lower stratosphere. Elsewhere, differences are typically within $\sim$5 ppbv, with localized differences up to $\sim$15 ppbv.

- MLS v2.2 and ACE H_2O agree very well throughout the stratosphere, typically within 5%. HALOE H_2O shows a persistent low bias with respect to MLS of $\sim$5–10%, consistent with previous studies.

- MLS v2.2 and ACE CO compare very well qualitatively, and overall quantitatively; however, MLS CO is noisy and still contains some vertical oscillations in the stratosphere that compromise detailed quantitative agreement.

- MLS v2.2 and ACE HNO_3 agree very well qualitatively, and to within 5-20% in the region surrounding the peak, $\sim$550 to 900 K. At higher and lower levels, MLS shows a low bias with respect to ACE.

- MLS v2.2 and ACE HCl agree well throughout the stratosphere; HALOE HCl is $\sim$5–25% lower than MLS and ACE.

In addition, comparisons of SO with v2.2 MLS O_3 at the tropopause agree well between all of the instruments. These results are consistent with more conventional validation results presented in other papers in this issue, and help to extend those results to a broader range of conditions.

Further work to add to and improve DMPs is planned, including calculating DMPs for all SO datasets from GEOS-4 (and GEOS-5 when that reanalysis is complete) data, and calculating DMPs for SAGE I and possibly for other datasets, such as UARS MLS and UARS Cryogenic Limb Array Etalon Spectrometer. We hope to continue operational production of the DMPs for MLS and ACE for the duration of those missions. A procedure is available for users to request DMPs calculated at locations that they define (see Appendix); the system for this is being used to produce DMPs for ACE validation campaigns [e.g., *Walker et al.*, 2005; *Kerzenmacher et al.*, 2005] conducted in Eureka in 2004 through 2007 and planned for 2008. We are using the DMPs in several studies combining SO datasets and MLS data, and hope that they will be useful to other researchers in similar efforts.

Appendix: DMP Access, File Format, and Usage

Table 3 shows the locations for SO DMP access via anonymous ftp from mls.jpl.nasa.gov; these can also be accessed from the MLS webpage (http://mls.jpl.nasa.gov) under http://mls.jpl.nasa.gov/research/meteorology.php. The ACE DMPs are provided to the ACE Science Team and distributed by them. For information on these products, please contact ACE Mission Scientist Peter Bernath (info@acebox.uwaterloo.ca).

DMPs can also be obtained by request at user-defined (UD) times/locations; see http://mls.jpl.nasa.gov/docs/genericDMPdescription.txt for information on how to make such a request and the format for the input files.

Aura MLS DMPs are publicly available at http://mls.jpl.nasa.gov/dmp. Users must first request access and agree not to redistribute the MLS DMP files. This access request is not intended as a restriction, but rather as a means to gauge community uses for these products and to provide users with updates and information on changes or problems. MLS DMPs can be downloaded for v1.5 and v2.2, GEOS-4 or 5 and MetO, for the full Aura mission.

The formats of the DMP files are designed to follow as closely as possible the formats of the datasets they are provided for. Information on the file formats and links to sample read software are provided on the ftp or web sites along with the DMPs.

References

Allen, D. R., J. L. Stanford, M. A. López-Valverde, N. Nakamura, D. J. Lary, A. R. Douglass, M. C. Cerniglia, J. J. Remedios, and F. W. Taylor (1999), Observations of middle atmosphere CO from the UARS ISAMS during the early northern winter 1991/1992, *J. Atmos. Sci.*, *56*, 563–583.

Barrett, B., et al. (2006), Intercomparisons of trace gas profiles from the Odin/SMR and Aura/MLS limb sounders, *J. Geophys. Res.*, *111*, D21,302, doi:10.1029/2006JD007,305, 2006.

Bernath, B. F., et al. (2005), Atmospheric Chemistry Experiment (ACE): mission overview, *Geophys. Res. Lett.*, *32*, L15S01, doi:10.1029/2005GL022,386.

Bethan, S., G. Vaughan, and S. J. Reid (1996), A comparison of ozone and thermal tropopause heights and the impact of tropopause definition on quantifying the ozone content of the troposphere, *Q. J. R. Meteorol. Soc.*, *122*, 929–944.

Bloom, S. C., L. L. Takacs, A. M. da Silva, and D. Ledvina (1996), Data assimilation using incremental analysis updates, *Mon. Weather Rev.*, *124*, 1256–1271.

Bloom, S. C., et al. (2005), The Goddard Earth Observing Data Assimilation System, GEOS DAS Version 4.0.3: Documentation and validation, *Tech. Rep. 104606 V26*, NASA.

Boone, C. D., R. Nassar, K. A. Walker, Y. Rochon, S. D. McLeod, C. P. Rinsland, and P. F. Bernath (2005), Retrievals for the Atmospheric Chemistry Experiment Fourier-Transform Spectrometer, *Appl. Opt.*, *44*, 7218–7231.

Borchi, F., and J.-P. Pommereau (2006), Evaluation of ozonesondes, HALOE, SAGE II and III, Odin-OSIRIS and SMR, and ENVISAT-GOMOS, -SCIAMACHY and -MIPAS ozone profiles in the tropics from SAOZ long duration balloon measurements in 2003 and 2004, *Atmos. Chem. Phys. Disc.*, *6*, 10,087–10,152.

Braathen, G., et al. (2006), Joint WMO/EU Arctic ozone bulletin, winter/spring summary, *Tech. Rep. 2006-1*, World Meteorological Organization/European Ozone Research Coordinating Unit.

Butchart, N., and E. E. Remsberg (1986), The area of the stratospheric polar vortex as a diagnostic for tracer transport on an isentropic surface, *J. Atmos. Sci.*, *43*, 1319–1339.

Chu, W. P., M. P. McCormick, J. Lenoble, C. Brogniez, and P. Pruvost (1989), SAGE II inversion algorithm, *J. Geophys. Res.*, *94*, 8339–8351.

Clerbaux, C., P.-F. Coheur, D. Hurtmans, B. Barret, M. Carleer, K. Semeniuk, J. C. McConnell, C. Boone, and P. Bernath

Table 3. Availability of SO Instrument DMPs via FTP

Mission/Instrument	Location[1]	Types	Time range
ACE-FTS	Distributed by ACE team	MetO, GEOS{4,5}	2004/01–present
SAGE II[2]	sage2/dmp/v5.0	NCEP/CPC	1984/10-2005/08
	sage2/dmp/v5.0	MetO	1991/10-2005/08
SAGE III[2]	sage3/v03.00/dmp/g3asmb/v1.1/<y>/<d>[3]	MetO	2002/05–2005/12
POAM II[2]	poam2/v6.00/dmp/v1.0	MetO	1993/10–1996/11
POAM III[2]	poam3/v4.00/dmp/v1.0	MetO	1998/04–2005/12
HALOE	haloe/v19/dmp/v1.1/<y>	MetO	1991/10–2005/11

[1] Relative to pub/outgoing/manney after logging in via FTP
[2] Example software for reading SAGE II and III and POAM II and III DMPs can be found at
https://www.openchannelsoftware.com/projects/Example_IDL_Readers_for_DMPs
[3] <y>=4-digit year, <d>=3-digit day-of-year

(2005), Carbon monoxide distribution from the ACE-FTS solar occultation measurements, *Geophys. Res. Lett.*, *32*, L16S01, doi:10.1029/2005GL022,394.

Cunnold, D. M., W. P. Chu, R. A. Barnes, M. P. McCormick, and R. E. Veiga (1989), Validation of SAGE II ozone measurements, *J. Geophys. Res.*, *94*, 8447–8460.

Davies, T., M. J. P. Cullen, A. J. Malcolm, M. H. Mawson, A. Staniforth, A. A. White, and N. Wood (2005), A new dynamical core for the met office's global and regional modelling of the atmosphere, *Q. J. R. Meteorol. Soc.*, *131*, 1759–1782.

Derber, J. C., and W. Wu (1998), The use of TOVS cloud-cleared radiances in the NCEP SSI analysis system, *Mon. Weather Rev.*, *126*, 2287–2299.

Dufour, G., et al. (2005), Partitioning between the inorganic chlorine reservoirs HCl and ClONO$_2$ during the Arctic winter 2005 derived from the ACE-FTS measurements, *Atmos. Chem. Phys.*, *6*, 2355–2366.

Dunkerton, T. J., and D. P. Delisi (1986), Evolution of potential vorticity in the winter stratosphere of January-February 1979, *J. Geophys. Res.*, *91*, 1199–1208.

Filipiak, M. J., et al. (2005), Carbon monoxide measured by the EOS Microwave Limb Sounder on Aura: First results, *Geophys. Res. Lett.*, *32*, L14,825, doi:10.1029/2005GL022,765.

Finger, F. G., H. M. Woolf, and C. E. Anderson (1965), A method for objective analysis of stratospheric constant pressure charts, *Mon. Weather Rev.*, *93*, 619–638.

Finger, F. G., M. E. Gelman, J. D. Wild, M. L. Chanin, A. Hauchecorne, and A. J. Miller (1993), Evaluation of NMC upper-stratospheric temperature analyses using rocketsonde and lidar data, *Bull. Am. Meteorol. Soc.*, *74*, 789–799.

Froidevaux, L., et al. (2006), Early validation analyses of atmospheric profiles from EOS MLS on the Aura satellite, *IEEE Trans. Geosci. Remote Sens.*, *44*, 1106–1121.

Froidevaux, L., et al. (2007a), Validation of EOS MLS HCl measurements, *J. Geophys. Res.*, submitted, 2007.

Froidevaux, L., et al. (2007b), Validation of EOS MLS stratospheric ozone measurements, *J. Geophys. Res.*, submitted, 2007.

Fussen, D., F. Vanhellemont, J. Dodion, C. Bingen, K. A. Walker, C. D. Boone, S. D. McLeod, and P. F. Bernath (2005), Initial intercomparison of ozone and nitrogen dioxide number density profiles retrieved by the ACE-FTS and GOMOS

occultation experiments, *Geophys. Res. Lett.*, *32*, L16S02, doi:10.1029/2005GL022,468.

Gelman, M. E., A. J. Miller, K. W. Johnson, and R. M. Nagatani (1986), Detection of long term trends in global stratospheric temperature from NMC analyses derived from NOAA satellite data, *Adv. Space. Res.*, *6(10)*, 17–26.

Gelman, M. E., A. J. Miller, R. M. Nagatani, and C. S. Long (1994), Use of UARS data in the NOAA stratospheric monitoring program, *Adv. Space. Res.*, *14(9)*, 21–31.

Glaccum, W., , et al. (1996), The Polar Ozone and Aerosol Measurement instrument, *J. Geophys. Res.*, *101*, 14,479–14,487.

Harvey, V. L., R. B. Pierce, M. H. Hitchman, C. E. Randall, and T. D. A. Fairlie (2004), On the distribution of ozone in stratospheric anticyclones, *J. Geophys. Res.*, *109*, D24308, doi:10.1029/2004JD004992.

Highwood, E. J., and P. Berrisford (2000), Properties of the Arctic tropopause, *Q. J. R. Meteorol. Soc.*, *126*, 1515–1532.

Jiang, Y., et al. (2007), Aura Microwave Limb Sounder validation by ozonesonde and lidar measurements, *J. Geophys. Res.*, submitted, 2007.

Jin, J. J., et al. (2006), Denitrification in the Arctic winter 2004/2005: Observations from ACE-FTS, *Geophys. Res. Lett.*, *33*, L19,814, doi:10.1029/2006GL027,687.

Kerzenmacher, T. E., et al. (2005), Measurements of O$_3$, NO$_2$ and temperature during the 2004 Canadian Arctic ACE validation campaign, *Geophys. Res. Lett.*, *32*, L16S07, doi:10.1029/2005GL023,032.

Kley, D., et al. (2000), SPARC assessment of upper tropospheric and stratospheric water vapour, *Tech. Rep. SPARC Report No. 2*, WCRP-No. 113, WMO/TD-No, 104.

Lait, L. R., et al. (1990), Reconstruction of O$_3$ and N$_2$O fields from ER-2, DC-8, and balloon observations, *Geophys. Res. Lett.*, *17*, 521–524.

Lambert, A., et al. (2007), Validation of the Aura Microwave Limb Sounder stratospheric water vapor and nitrous oxide measurements, *J. Geophys. Res.*, submitted, 2007.

Livesey, N. J., et al. (2005), Version 1.5 level 2 data quality and description document, *Tech. Rep. JPL D-32381*, Jet Propulsion Laboratory.

Lorenc, A. C., R. S. Bell, and B. Macpherson (1991), The Meteorological Office analysis correction data assimilation scheme, *Q. J. R. Meteorol. Soc.*, *117*, 59–89.

Lorenc, A. C., et al. (2000), The Met. Office global three-dimensional variational data assimilation scheme, *Q. J. R. Meteorol. Soc.*, *126*, 2991–3012.

Lucke, R. L., et al. (1999), The Polar Ozone and Aerosol Measurement (POAM) III instrument and early validation results, *J. Geophys. Res.*, *104*, 18,785–18,799.

Lumpe, J. D., et al. (2002), POAM III retrieval algorithm and error analysis, *J. Geophys. Res.*, *107*, doi:10.1029/2002JD002,137.

Lumpe, J. D., et al. (2003), Comparison of POAM III ozone measurments with correlative aircraft and balloon data during SOLVE, *J. Geophys. Res.*, *108*, 8316, doi:10.1029/2001JD000,472.

Lumpe, J. D., et al. (2006), Validation of Polar Ozone and Aerosol Measurement (POAM) III version 4 stratospheric water vapor, *J. Geophys. Res.*, *111*, D11,301, doi:10.1029/2005JD006,763.

Mann, G. W., S. Davies, K. S. Carslaw, M. P. Chipperfield, and J. Kettleborough (2002), Polar vortex concentricity as a controlling factor in Arctic denitrification, *J. Geophys. Res.*, *107*, 4663 doi:10.1029/2002JD002,102.

Manney, G. L., R. W. Zurek, M. E. Gelman, A. J. Miller, and R. Nagatani (1994a), The anomalous Arctic lower stratospheric polar vortex of 1992–1993, *Geophys. Res. Lett.*, *21*, 2405–2408.

Manney, G. L., R. W. Zurek, A. O'Neill, and R. Swinbank (1994b), On the motion of air through the stratospheric polar vortex, *J. Atmos. Sci.*, *51*, 2973–2994.

Manney, G. L., L. Froidevaux, J. W. Waters, and R. W. Zurek (1995a), Evolution of Microwave Limb Sounder ozone and the polar vortex during winter, *J. Geophys. Res.*, *100*, 2953–2972.

Manney, G. L., M. L. Santee, L. Froidevaux, J. W. Waters, and R. W. Zurek (1996a), Polar vortex conditions during the 1995–96 Arctic winter: Meteorology and MLS ozone, *Geophys. Res. Lett.*, *23*, 3203–3206.

Manney, G. L., R. Swinbank, S. T. Massie, M. E. Gelman, A. J. Miller, R. Nagatani, A. O'Neill, and R. W. Zurek (1996b), Comparison of U. K. Meteorological Office and U. S. National Meteorological Center stratospheric analyses during northern and southern winter, *J. Geophys. Res.*, *101*, 10,311–10,334.

Manney, G. L., H. A. Michelsen, M. L. Santee, M. R. Gunson, F. W. Irion, A. E. Roche, and N. J. Livesey (1999), Polar vortex dynamics during spring and fall diagnosed using trace gas observations from the Atmospheric Trace Molecule Spectroscopy instrument, *J. Geophys. Res.*, *104*, 18,841–18,866.

Manney, G. L., H. A. Michelsen, F. W. Irion, M. R. Gunson, G. C. Toon, and A. E. Roche (2000), Lamination and polar vortex development in fall from ATMOS long-lived trace gases observed during November 1994, *J. Geophys. Res.*, *105*, 29,023–29,038.

Manney, G. L., W. A. Lahoz, J. L. Sabutis, A. O'Neill, and L. Steenman-Clark (2002), Simulations of fall and early winter in the stratosphere, *Q. J. R. Meteorol. Soc.*, *128*, 2205–2237.

Manney, G. L., J. L. Sabutis, S. Pawson, M. L. Santee, B. Naujokat, R. Swinbank, M. E. Gelman, and W. Ebisuzaki (2003), Lower stratospheric temperature differences between meteorological analyses in two cold Arctic winters and their impact on polar processing studies, *J. Geophys. Res.*, *108*, 8328, doi:10.1029/2001JD001,149.

Manney, G. L., M. L. Santee, N. J. Livesey, L. froidevaux, W. G. Read, H. C. Pumphrey, J. W. Waters, and S. Pawson (2005a), EOS Microwave Limb Sounder observations of the Antarctic polar vortex breakup in 2004, *Geophys. Res. Lett.*, *32*, L12,811, doi:10.1029/2005GL022,823.

Manney, G. L., M. L. Santee, L. Froidevaux, K. Hoppel, N. J. Livesey, and J. W. Waters (2006), EOS MLS observations of ozone loss in the 2004-2005 Arctic winter, *Geophys. Res. Lett.*, *33*, L04,802, doi:10.1029/2005GL024,494.

Manney, G. L., et al. (1995b), Formation of low-ozone pockets in the middle stratospheric anticyclone during winter, *J. Geophys. Res.*, *100*, 13,939–13,950.

Manney, G. L., et al. (2001), Comparison of satellite ozone observations in coincident air masses in early November 1994, *J. Geophys. Res.*, *106*, 9923–9944.

Manney, G. L., et al. (2005b), Diagnostic comparison of meteorological analyses during the 2002 Antarctic winter, *Mon. Weather Rev.*, *133*, 1261–1278.

Mauldin, L. E., N. H. Zaun, M. P. McCormick, J. H. Guy, and W. R. Vaugh (1985), Stratospheric Aerosol and Gas Experiment II instrument: A functional description, *Opt. Eng.*, *24*, 307–312.

McCormick, M. P., J. M. Zawodny, R. E. Veiga, J. C. Larsen, and P. H. Wang (1989), An overview of SAGE I and SAGE II ozone measurements, *Planet. Space Sci.*, *37*, 1567–1586.

McCormick, M. P., et al. (2002), SAGE III algorithm theoretical basis document: Solar and lunar algorithm, *Tech. Rep. 475-00-108, Version 2.1*, NASA Langley Research Center.

McNally, A. P., J. C. Derber, W. Wu, and B. B. Katz (2000), The use of TOVS level-1b radiances in the NCEP SSI analysis system, *Q. J. R. Meteorol. Soc.*, *126*, 689–724.

Michelsen, H. A., et al. (2002), ATMOS version 3 water vapor measurements: Comparisons with ATMOS version 2 retrievals and observations from two ER-2 Lyman-α hygrometers, MkIV, MAS, HALOE, and MLS, *J. Geophys. Res.*, *107*, 10.1029/2001JD000,587.

Nash, E. R., P. A. Newman, J. E. Rosenfield, and M. R. Schoeberl (1996), An objective determination of the polar vortex using Ertel's potential vorticity, *J. Geophys. Res.*, *101*, 9471–9478.

Nassar, R., P. F. Bernath, C. D. Boone, G. L. Manney, S. D. McLeod, C. P. Rinsland, R. Skelton, and K. A. Walker (2005), Stratospheric abundances of water and methane based on ACE-FTS measurements, *Geophys. Res. Lett.*, *32*, L15S04, doi:10.1029/2005GL022,383.

Newman, P. A., L. R. Lait, M. R. Schoeberl, R. M. Nagatani, and A. J. Krueger (1989), Meteorological atlas of the Northern Hemisphere lower stratosphere for January and February 1989 during the Airborne Arctic Stratospheric Expedition, *Tech. Rep. 4145*, NASA.

Orsolini, Y. J., C. E. Randall, G. L. Manney, and D. R. Allen (2005), An observational study of the final breakdown of the southern hemisphere stratospheric vortex in 2002, *J. Atmos. Sci.*, *62*, 735–747.

Pan, L., S. Solomon, W. Randel, J. F. Lamarque, P. Hess, J. Gille, E. W. Chiou, and M. P. McCormick (1997), Hemispheric asymmetries and seasonal variations of the lowermost stratospheric water vapor and ozone deprived from SAGE II data, *J. Geophys. Res.*, *102*, 28,117–28,184.

Pawson, S., et al. (2007), Goddard Earth Observing System analyses for EOS-Aura, *J. Geophys. Res., submitted*, 2007.

Petelina, S. V., et al. (2005), Validation of ACE-FTS stratospheric ozone profiles against Odin/OSIRIS measurements, *Geophys. Res. Lett., 32*, L15S06, doi:10.1029/2005GL022,377.

Pumphrey, H. C., et al. (2007), Validation of the Aura Microwave Limb Sounder stratospheric and mesospheric CO measurements, *J. Geophys. Res.*, submitted, 2007.

Randall, C. E., et al. (2003), Validation of POAM III ozone: Comparisons with ozonesonde and satellite data, *J. Geophys. Res., 108*, 4367, doi:10.1029/2002JD002,944.

Randall, C. E., et al. (2005), Stratospheric effects of energetic particle precipitation in 2003-2004, *Geophys. Res. Lett., 32*, L05,802, doi:10.1029/2004GL022,003.

Randel, W. J. (1987), The evaluation of winds from geopotential height data in the stratosphere, *J. Atmos. Sci., 44*, 3097–3120.

Randel, W. J., F. Wu, J. M. Russell, III, and J. W. Waters (1999), Space-time patterns of trends in stratospheric constituents derived from UARS measurements, *J. Geophys. Res., 104*, 3711–3727.

Redaelli, G., et al. (1994), UARS MLS O3 soundings compared with lidar measurements using the conservative coordinates reconstruction technique, *Geophys. Res. Lett., 21*, 1535–1538.

Reichler, T., M. Dameris, and R. Sausen (2003), Determining the tropopause height from gridded data, *Geophys. Res. Lett., 30*, 2042, doi:10.1029/2003GL018,240.

Reinecker, M. M., et al. (2007), The GEOS-5 data assimilation system: A documentation of GEOS-5.0, *Tech. Rep. 104606 V27*, NASA.

Remsberg, E., et al. (2002), An assessment of the quality of HALOE temperature profiles in the mesosphere based on comparisons with Rayleigh backscatter lidar and inflatable falling sphere measurements, *J. Geophys. Res., 107*, doi:10.1029/2001JD001,521.

Russell, J. M., III, et al. (1993), The Halogen Occultation Experiment, *J. Geophys. Res., 98*, 10,777–10,797.

Santee, M. L., G. L. Manney, N. J. Livesey, and W. G. Read (2004), Three-dimensional structure and evolution of stratospheric HNO3 based on UARS Microwave Limb Sounder measurements, *J. Geophys. Res., 109*, D15,306, doi:10.1029/2004JD004,578.

Santee, M. L., et al. (2007a), Validation of the Aura Microwave Limb Sounder ClO measurements, *J. Geophys. Res.*, submitted, 2007.

Santee, M. L., et al. (2007b), Validation of the Aura Microwave Limb Sounder HNO3 measurements, *J. Geophys. Res.*, submitted, 2007.

Schoeberl, M. R. (2004), Extratropical stratosphere-troposphere mass exchange, *J. Geophys. Res., 109*, D13,303, doi:10.1029/2004JD004,525.

Schoeberl, M. R., M. Luo, and J. E. Rosenfield (1995), An analysis of the Antarctic Halogen Occultation Experiment trace gas observations, *J. Geophys. Res., 100*, 5159–5172.

Schoeberl, M. R., et al. (2006), Chemical observations of a polar vortex intrusion, *J. Geophys. Res., 111*, D20,306, doi:10.1029/2006JD007,134.

Schwartz, M. J., et al. (2007), Validation of the Aura Microwave Limb Sounder temperature and geopotential height measurements, *J. Geophys. Res.*, submitted, 2007.

Singleton, C. S., et al. (2007), Quantifying Arctic ozone loss during the 2004-2005 winter using satellite observations and a chemical transport model, *J. Geophys. Res.*, in press, 2007.

Solomon, S. (1999), Stratospheric ozone depletion: A review of concepts and history, *Rev. Geophys., 37*, 275–316.

Solomon, S., R. R. Garcia, J. J. Olivero, R. M. Bevilacqua, P. R. Schwartz, R. T. Clancy, and D. O. Muhleman (1985), Photochemistry and transport of carbon monoxide in the middle atmosphere, *J. Atmos. Sci., 42*, 1072–1083.

Stajner, I., C. Benson, H. C. Liu, S. Pawson, N. Brubaker, L.-P. Chang, L. P. Riishojgaard, and R. Todling (2007), Ice polar stratospheric clouds detected from assimilation of atmospheric infrared sounder data, *Geophys. Res. Lett.*, submitted, 2007.

Swinbank, R., and A. O'Neill (1994), A stratosphere-troposphere data assimilation system, *Mon. Weather Rev., 122*, 686–702.

Swinbank, R., N. B. Ingleby, P. M. Boorman, and R. J. Renshaw (2002), A 3D variational data assimilation system for the stratosphere and troposphere, *Tech. Rep. 71*, Met Office Numerical Weather Prediction Forecasting Research Scientific Paper.

Swinbank, R., M. Keil, D. R. Jackson, and A. A. Scaife (2004), Stratospheric data assimilation at the Met Office - progress and plans, in *ECMWF workshop on Modelling and Assimilation for the Stratosphere and Tropopause 23-26-June, 2003*, ECMWF.

Taha, G., L. W. Thomason, and S. P. Burton (2004), Comparison of stratospheric aerosol and gas experiment (SAGE) II version 6.2 water vapor with balloon-borne and space-based instruments, *J. Geophys. Res., 109*, D18,313, doi:10.1029/2004JD004,859.

Thomason, L. W., L. R. Poole, and C. E. Randall (2006), SAGE III aerosol extinction validation in the Arctic winter: comparisons with SAGE II and POAM III, *Atmos. Chem. Phys. Disc., 2006, No. 6*, 11,357–11,389.

Walker, K. A., C. E. Randall, C. R. Trepte, C. D. Boone, and P. F. Bernath (2005), Initial validation comparisons for the Atmospheric Chemistry Experiment (ACE), *Geophys. Res. Lett., 32*, L16S04, doi:10.1029/2005GL022,388.

Wang, H.-J., D. M. Cunnold, L. W. Thomason, J. M. Zawodny, and G. E. Bodeker (2002), Assessment of SAGE version 6.1 ozone data quality, *J. Geophys. Res., 107*, 4691, doi:10.1029/2002JD002,418.

Wang, H.-J., D. M. Cunnold, C. Trepte, L. W. Thomason, and J. M. Zawodny (2006), SAGE III solar ozone measurements: Initial results, *Geophys. Res. Lett., 33*, L03,805, doi:10.1029/2005GL025,099.

Waters, J. W., et al. (2006), The Earth Observing System Microwave Limb Sounder (EOS MLS) on the Aura satellite, *IEEE Trans. Geosci. Remote Sens., 44*, 1075–1092.

WMO (2007), Scientific assessment of stratospheric ozone depletion: 2006, U. N. Environ. Program, Geneva, Switzerland.

Wu, W.-S., R. J. Purser, and D. F. Parish (2002), Three-dimensional variational analyses with spatially inhomogeneous covariances, *Mon. Weather Rev., 130*, 2905–2916.

Gloria L. Manney, Mail Stop 183-701. Jet Propulsion Laboratory, California Institute of Technology, Pasadena, CA 91109, USA, Gloria.L.Manney@jpl.nasa.gov
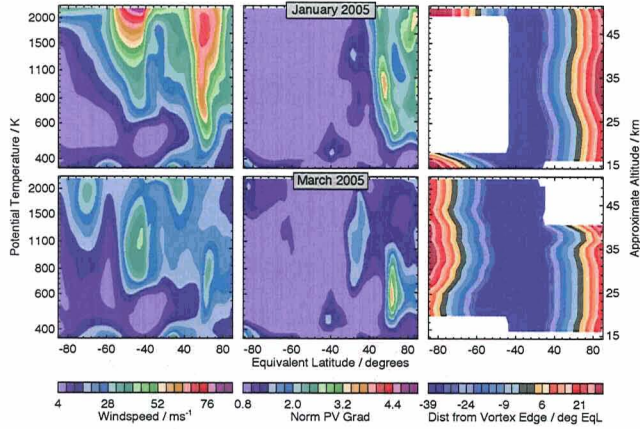
Figure 1. Monthly averages of equivalent latitude (EqL)/potential temperature (θ)-mapped (left to right) windspeed (ms^{-1}), normalized (see text) horizontal PV gradient, and distance in EqL from the vortex edge center ($^\circ$EqL). EqL/θ mapping is from derived meteorological products (DMPs) calculated from GEOS-4 data for MLS locations, during (top) January 2005 and (bottom) March 2005. White space in EqL from vortex edge plots indicates that the vortex is not defined anytime during the month in these regions.
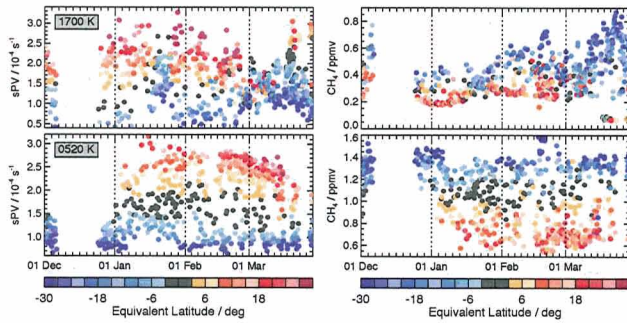
Figure 2. Timeseries of distance in EqL from vortex edge center (colors, $^\circ$EqL) as a function of (left) sPV (10^{-4} s^{-1}) and (right) ACE CH$_4$ (ppmv) at (top) 1700 K and (bottom) 520 K, for ACE measurement locations during December through March 2005. Vortex edge location values are from GEOS-4 DMPs.
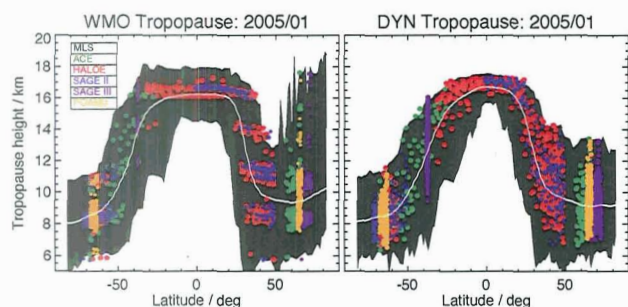
Figure 3. (Left) WMO and (right) dynamical (see text) tropopause altitudes from MetO DMPs for MLS (range shown as grey shading, white line average), ACE (green), HALOE (red), SAGE II (blue), SAGE III (purple) and POAM III (gold) for all measurements in January 2005. Tropopause pressures from MLS DMPs are converted to altitude using a scale height of 7.0 km.
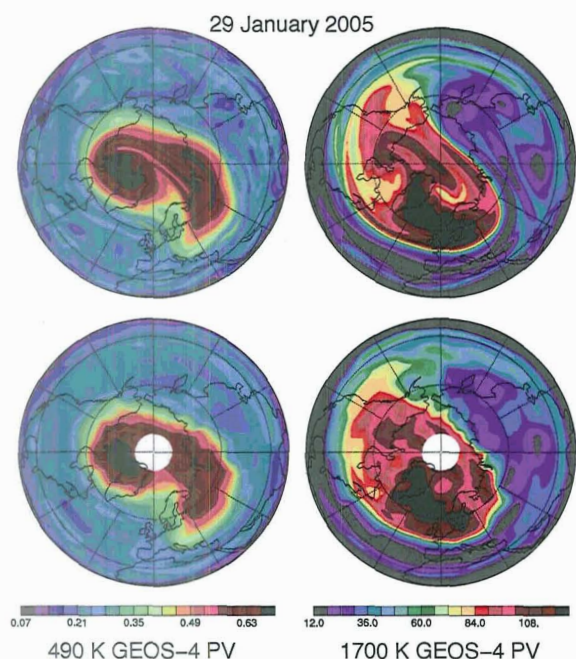
Figure 4. PV (10^{-4} K m^2 kg^{-1} s^{-1}) maps from GEOS-4 analyses (top row) and gridded (see text) from the MLS GEOS-4 DMP PV field (bottom row), at 490 K (left) and 1700 K (right). Projection is orthographic, with 0° longitude at the bottom; latitude range is from 0° to 90°N.
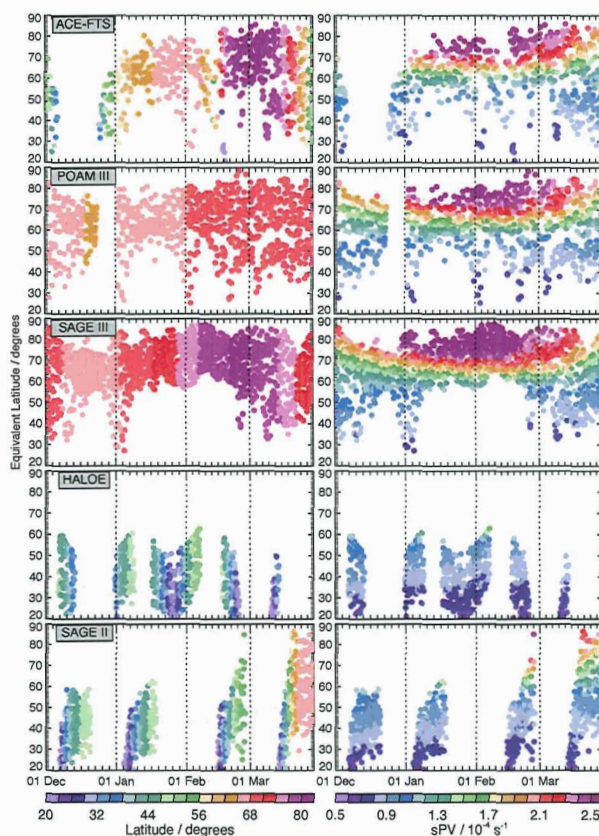
Figure 5. EqL/time plots of latitude (°, left) and sPV (10^{-4} s^{-1}) sampled by (top to bottom) ACE, POAM III, SAGE III, HALOE, and SAGE II during December 2004 through January 2005 EqL on the 490 K isentropic surface.
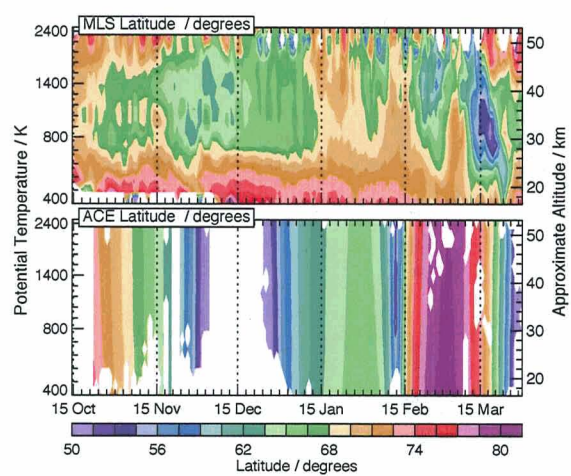
Figure 6. Vortex-averaged (within the 1.4×10^{-4} s^{-1} sPV contour from GEOS-4 DMPs) latitude (°) sampled by (top) MLS and (bottom) ACE from 15 October 2004 through 31 March 2005.
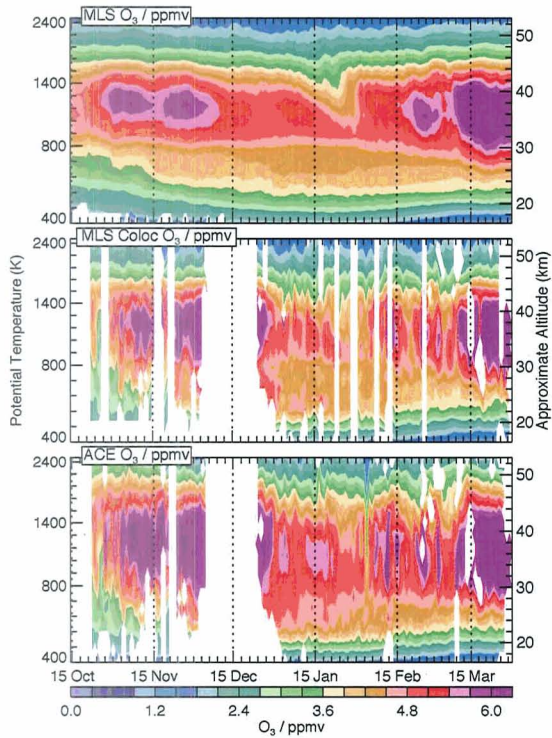
Figure 8. Vortex-averaged (within 1.4×10^{-4} s^{-1} sPV contour from GEOS-4 DMPs) O$_3$ (ppmv) for 3 October 2004 through 31 March 2005 from (top) MLS v1.5, (center) MLS v1.5 measurements coincident with ACE (see text), and (bottom) ACE. Vertical range is 400 to 2500 K.
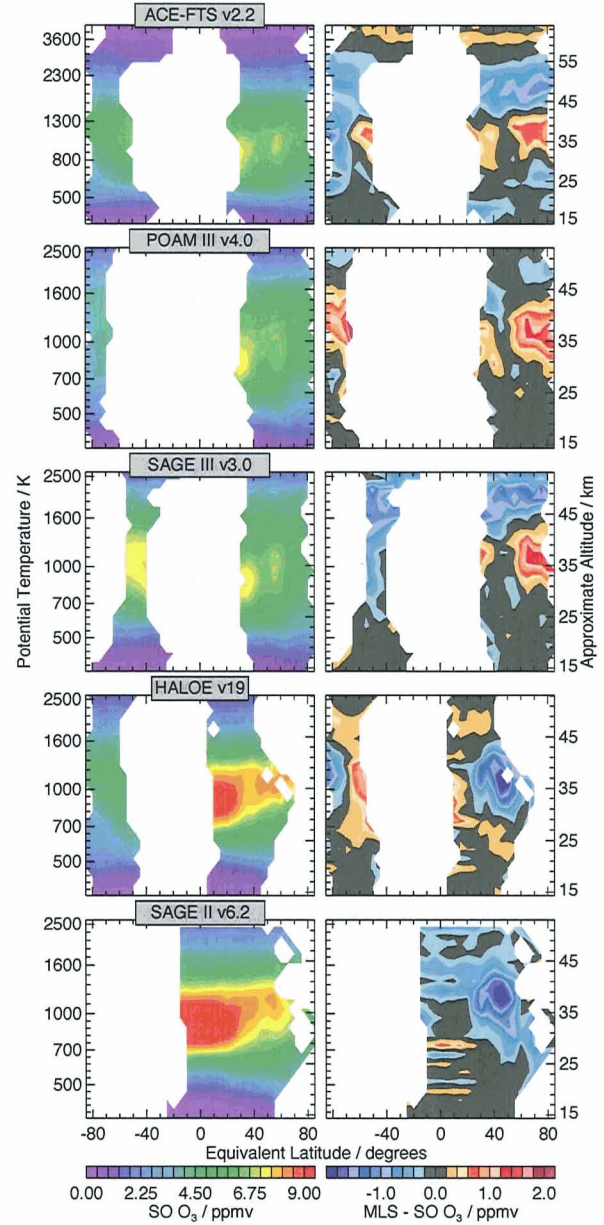
Figure 10. Global EqL/θ cross-sections for 10–16 March 2005 comparing MLS v2.2 O$_3$ with (top to bottom) ACE, POAM III, SAGE III, HALOE, and SAGE II. Left panels show the SO instruments' O$_3$ and right panels the MLS-SO instrument O$_3$ difference (ppmv). For MLS/ACE comparisons, GEOS-5 DMPs are used for EqL/θ mapping; others comparisons use MetO DMPs. MLS/ACE comparisons are shown from 360 through 4430 K; others are 360 through 2500 K (the top limit of the the MetO DMPs).
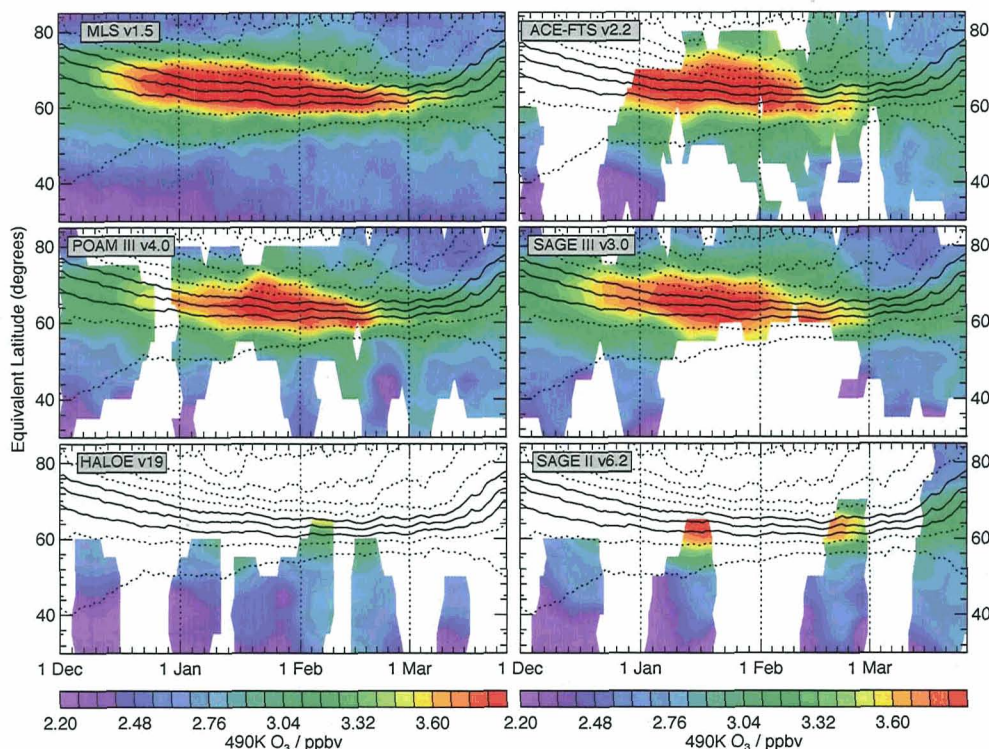
Figure 7. EqL/time series for 1 December 2004 through 31 March 2005 of O_3 (ppmv) at 490 K from (left to right, top to bottom) MLS (v1.5), ACE, POAM III, SAGE III, HALOE, and SAGE II. EqL mapping is done with MetO DMPs. Overlaid contours are sPV (10^{-4} s^{-1}), with three contours in the vortex edge region shown as solid lines.
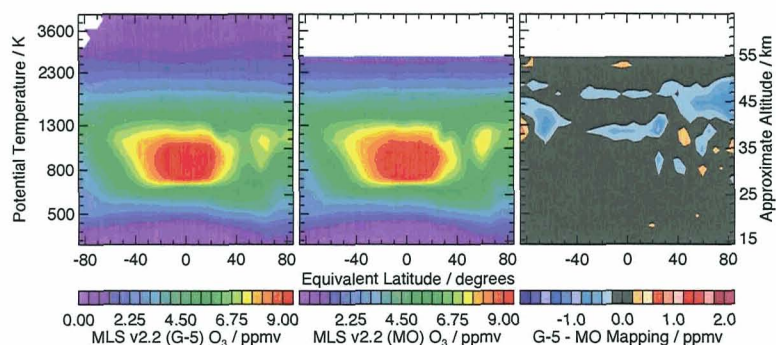
Figure 9. Global EqL/θ cross-sections for 10–16 March 2005 comparing MLS v2.2 O_3 (ppmv) mapped using GEOS-5 (left) and MetO (center) DMPs, and the difference (ppmv, right). Vertical range is 360 through 4300 K.
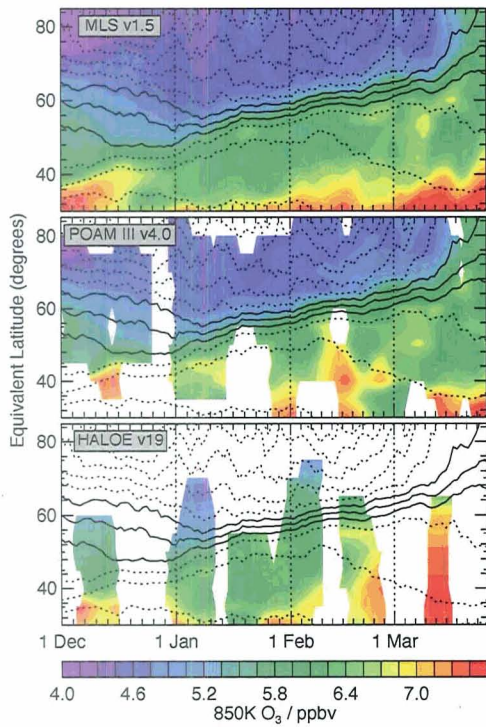
Figure 11. EqL/time series for 1 December 2004 through 31 March 2005 of O_3 (ppmv) at 850 K from (top to bottom) MLS (v1.5), POAM III, and HALOE. Mapping is done using MetO DMPs. Overlaid contours are sPV (10^{-4} s^{-1}), with three contours in the vortex edge region shown as solid lines.
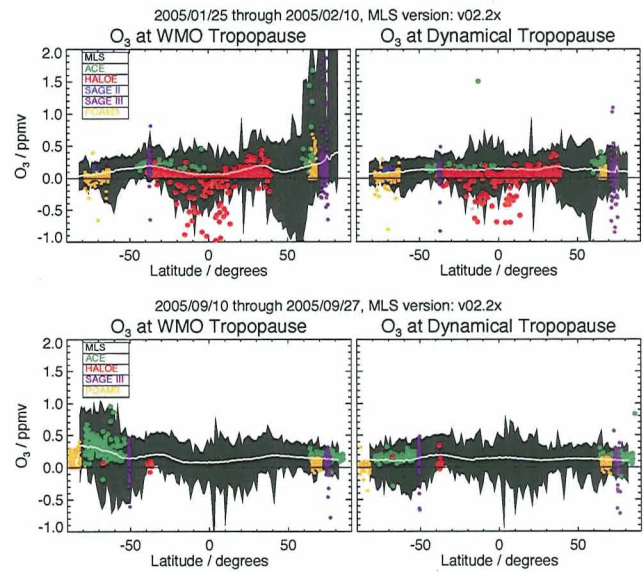
Figure 12. O_3 (ppmv) at the (left) WMO and (right) dynamical tropopause for MLS v2.2 (range shown as grey shading, average white line), ACE (green), HALOE (red), SAGE II (blue), SAGE III (purple) and POAM III (gold) for all measurements during (top) 24 January–10 February 2005 and (bottom) 10–27 September 2005. Tropopause locations for interpolation of O_3 are from MetO DMPs.
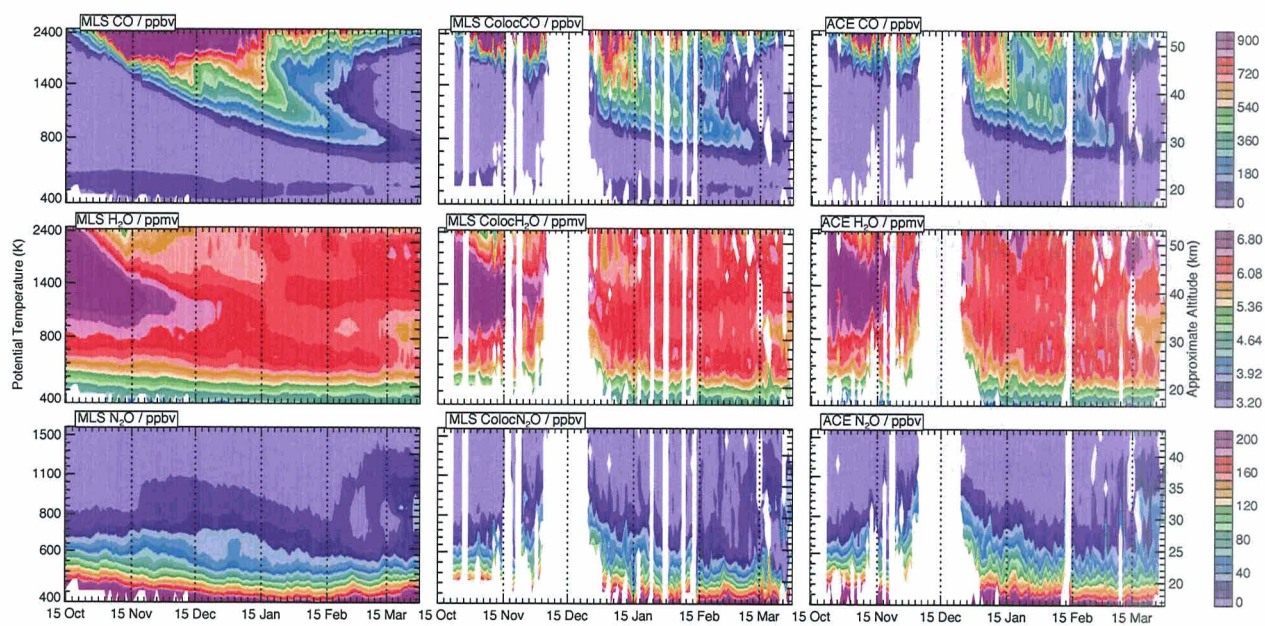
Figure 13. As in Figure 8, but for (top to bottom) CO (ppbv), H_2O (ppmv), and N_2O (ppbv). Vertical range for CO and H_2O is 400-2500 K; for N_2O, 400-1600 K. Vortex edge sPV is from GEOS-4 DMPs.
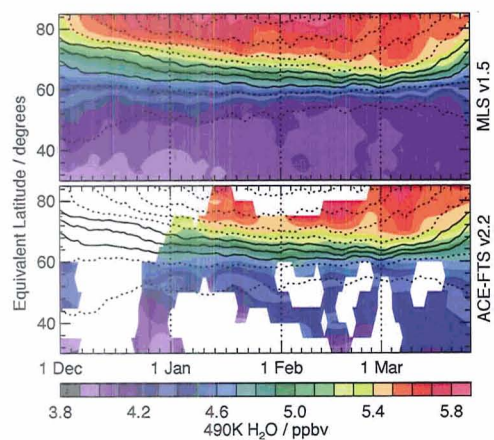
Figure 16. As in Figure 7, but for MLS v1.5 (top) and ACE (bottom) H$_2$O (ppmv) at 490 K, using GEOS-4 DMPs.
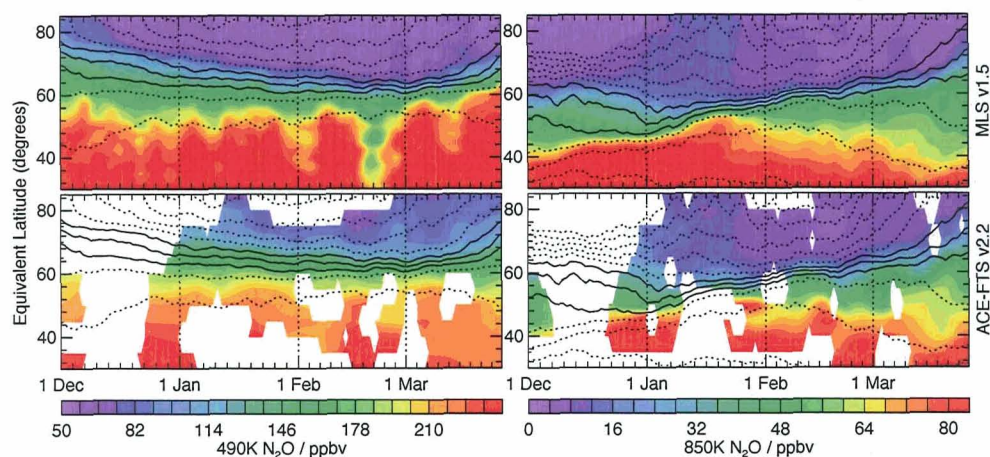
Figure 14. As in Figure 7, but for MLS v1.5 (top) and ACE (bottom) N_2O (ppbv) at (left) 490 and (right) 850 K, using GEOS-4 DMPs.
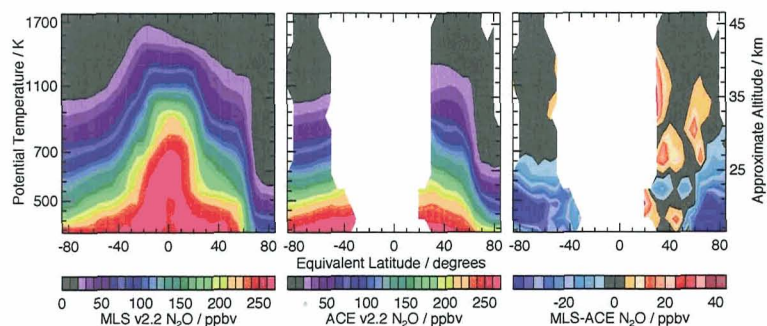
Figure 15. Global EqL/θ cross-sections for 10–16 March 2005 comparing MLS v2.2 with ACE N_2O Left panel shows MLS v2.2 N_2O, center panel, ACE N_2O, and right panel the MLS-ACE N_2O difference (ppbv). GEOS-5 DMPs are used for EqL/θ mapping. Vertical range is 400 through 1800 K.
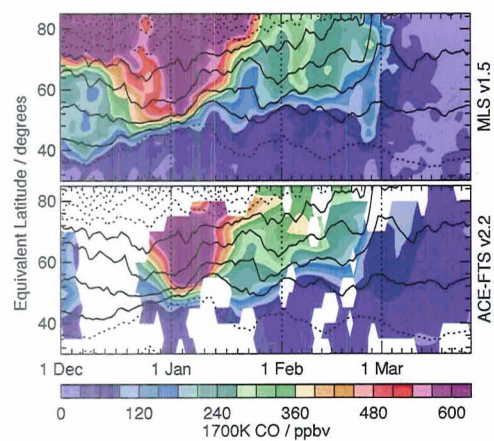
Figure 18. As in Figure 7, but for MLS v1.5 (top) and ACE (bottom) CO (ppbv) at 1700 K, using GEOS-4 DMPs.
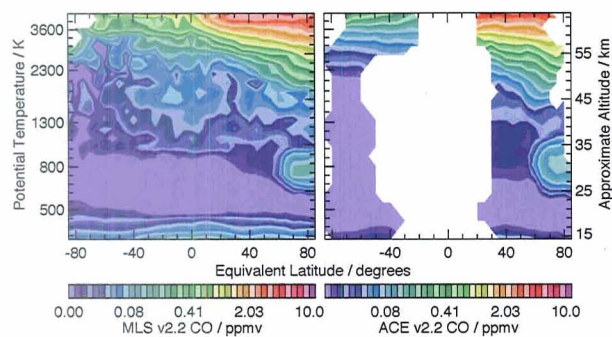
Figure 19. As in Figure 15 (with difference panel omitted), but for MLS v2.2 CO (ppbv) compared with ACE, using GEOS-5 DMPs. Vertical range is 360–4300 K. CO contour interval is on a log scale, from 20 to 10,000 ppbv.
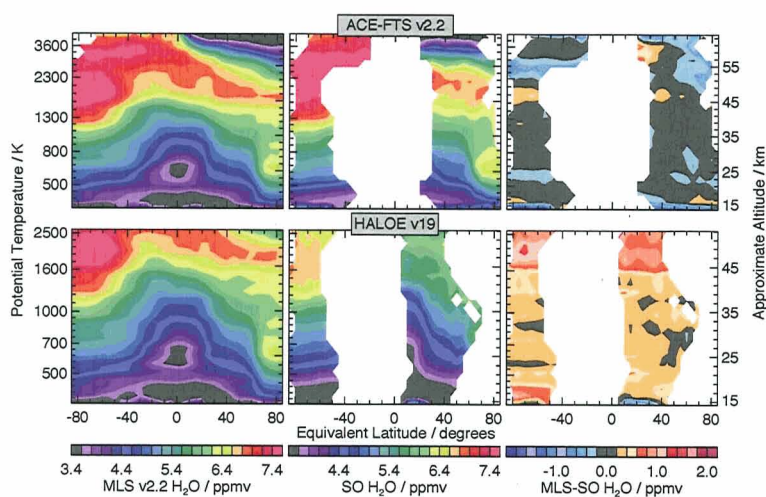
Figure 17. As in Figure 15, but for MLS v2.2 H$_2$O (ppmv) compared with (top) ACE and (bottom) HALOE. GEOS-5 DMPs are used for ACE comparison and MetO for HALOE comparison. Vertical range for ACE comparison is 360–4300 K, for HALOE comparison, 360–2500 K.
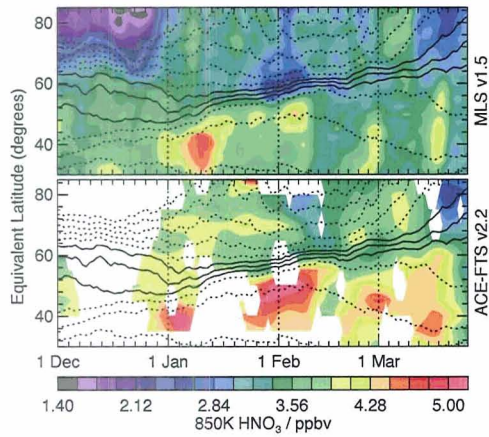
Figure 20. As in Figure 11, but for MLS v1.5 (top) and ACE (bottom) HNO₃ (ppbv) at 850 K, using GEOS-4 DMPs.
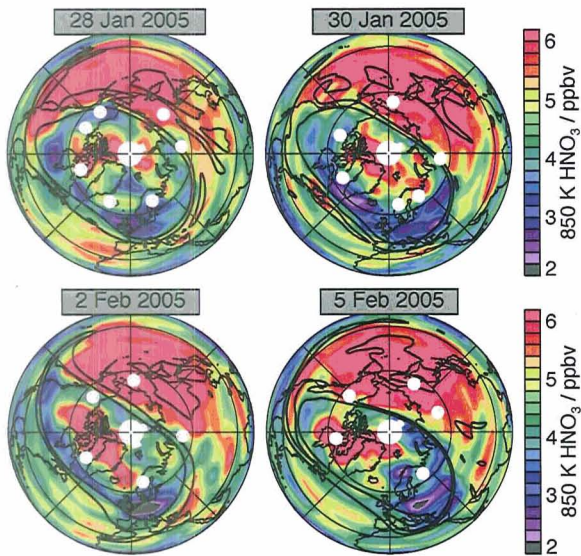
Figure 21. Maps of MLS v1.5 HNO₃ (ppbv) at 850 K for 28 and 30 January and 2 and 5 February 2005, with ACE observation locations (white dots) overlaid. PV contours in the vortex edge region are overlaid in black. Projection is orthographic, with 0° longitude at the bottom; latitude range is from 0 to 90°N.
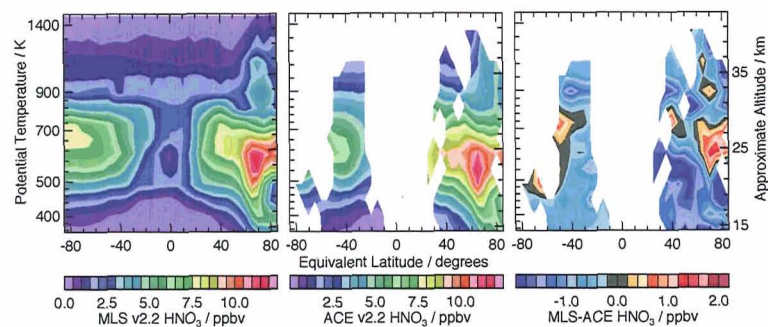
Figure 22. As in Figure 15, but for MLS v2.2 and ACE HNO$_3$ (ppbv) for 25–31 January 2005, using GEOS-5 DMPs. Vertical range is 400-1600 K.
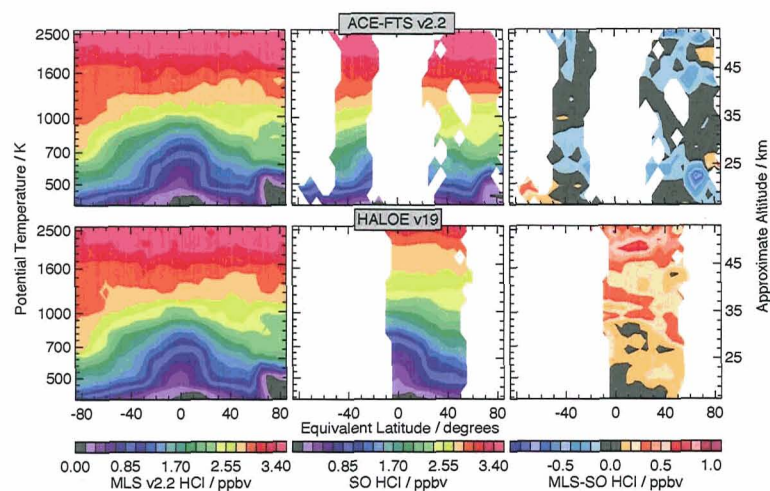
Figure 23. As in Figure 15, but for MLS v2.2, ACE, and HALOE HCl (ppbv) for 25–31 January 2005. ACE comparison uses GEOS-5 DMPs, HALOE comparison uses MetO DMPs. Vertical range is 400-2500 K.
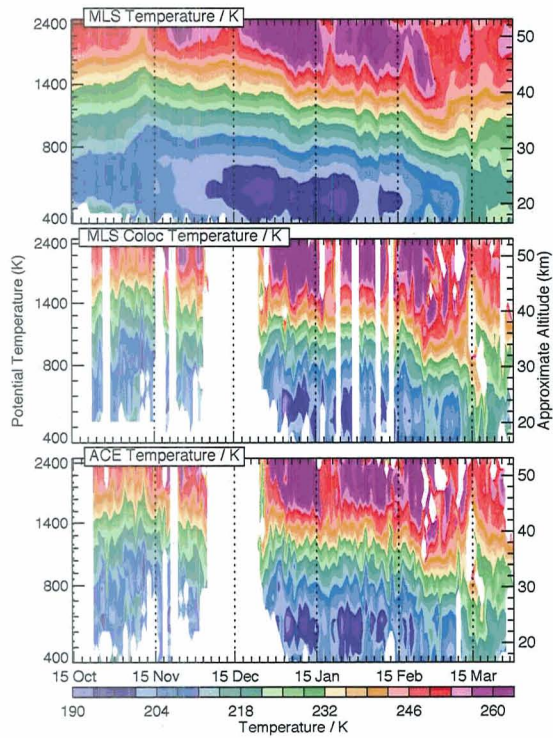
Figure 24. As in Figure 8, but for MLS v1.5 temperature (K). Vertical range is 400-2500 K. GEOS-4 DMPs are used to define the vortex edge.
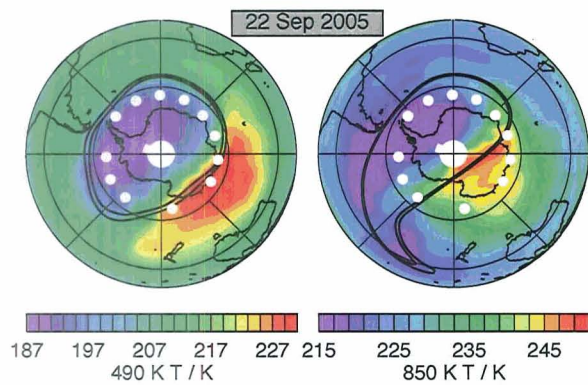

Figure 26. Maps of MLS v2.2 Temperature (colors, K) on 22 September 2005 at (left) 490 K and (right) 850 K. Overlaid contours are 1.4 and 1.8×10^{-4} s^{-1}. White dots show ACE observation locations.
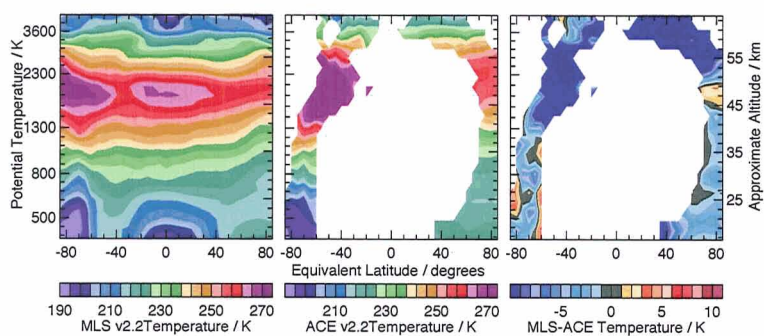
Figure 25. As in Figure 15, but for 17–24 September 2005 MLS v2.2 and ACE temperatures, using GEOS-5 DMPs. Vertical range is 360 to 4300 K.